Interrogation of Biological Samples by ToF-SIMS Using New Primary Ion Beams and Sample Preparation Methods

TINA B. ANGERER

UNIVERSITY OF GOTHENBURG

Department of Chemistry and Molecular Biology
University of Gothenburg
2017

DOCTORAL THESIS

Submitted for fulfilment of the requirements for the degree of
Doctor of Philosophy in Chemistry

Department of Chemistry and Molecular Biology
SE-412 96 Göteborg
Sweden
http://hdl.handle.net/2077/50294
ISBN 978-91-629-0073-1 (Print)
ISBN 978-91-629-0074-8 (PDF)

Printed by Ineko AB
Kållered, 2017

I. Abstract

Mass spectrometry is a very versatile and important technique in analytical chemistry. From atomic bombs to Alzheimer's disease, after a century of improvements and developments there are now countless applications for mass spectrometry in research and industry. One important branch within the field is imaging mass spectrometry as it combines chemical and location specific information.

Lipids, the main building blocks of cell membranes, are found in all living, cellular organisms. They are a diverse group of molecules, fulfilling structural and signal transduction functions. Right at the interface between the extra and intracellular environment, they are an important means of fast communication, they build a barrier to keep the cell alive, can promote cell death or indicate cellular changes in general. As different parts of organisms fulfil different functions, so is the distribution of lipids within organisms highly heterogeneous, indicating that each lipid has a role to play at its specific location.

To study the distribution of lipids, imaging time-of-flight secondary ion mass spectrometry (ToF-SIMS) is a well suited technique as it has a high sensitivity for detecting lipids and can detect lipid distributions on a sub-cellular scale in biological samples. As with any technique, ToF-SIMS has some drawbacks, for example it can be highly destructive so analysed lipids are fragmented and the molecular information is lost, there is a trade-off between spatial resolution and molecular information and the signal detected depends highly on the ionisation efficiency of different species, as well as their surroundings, which can skew the results. ToF-SIMS is a vacuum technique which presents challenges for biological sample handling and every analysis is only as good as the sample that is analysed.

To improve upon those aspects, getting more intact molecules at higher resolutions, improving sample preparation, work towards understating matrix effects and study the overall applicability of ToF-SIMS for biological samples was the scope of this thesis. Here I report my contribution to the field, how far we have come and what still needs to be done.

II. Populärvetenskaplig Sammanfattning

Vad och Var.

De frågor vi ställer i analytisk kemi kokar oftast ned till vad? och var? Vad orsakar att min processor i min dator inte fungerar? Vad består föroreningen av? Vad innehåller mitt läkemedel? Vart hamnar detta läkemedel i kroppen? Vilka förändringar orsakar läkemedlet in kroppen? Varifrån kommer dessa förändringar? Är förändringarna homogena? Detta är bara några exempel. Att veta vad som händer och var, är viktigt för att komma närmare till hur(!) någonting fungerar, så att vi kan förstå de händelser som händer inom och runt omkring oss. Bara när vi förstår, kan vi börja göra en förändring eller veta att vi faktisk har förändrat nånting, bota sjukdom, stoppa miljöförstöring och göra framsteg inom teknologin. Vissa analysmetoder kan komma på vad du har; andra var det är, bara några kan göra båda, imaging time-of-flight secondary ion mass spectrometry (ToF-SIMS) är en sådan metod.

ToF-SIMS gör det genom att analysera provet punkt för punkt (var!), och genererar masspektra för varje enskild punkt (vad!). genom metoden fås en kemisk karta som visar vad något är, var det är och hur mycket det är där. Är ToF-SIMS den perfekta analysmetoden? Nej, vi kan inte se allt vi vill se och vi får inte veta var något är, så exakt som vi vill veta. Kan vi lita på hur mycket det är? Nej, mestadels inte. Men tekniken förbättras hela tiden, och forskare, och som denna avhandling visar däribland jag, arbetar ständigt med att förbättra tekniken.

I denna avhandling berättar jag om betydelsen och varierande funktioner av lipider, en av livets byggstenar; beskriver vägen från fysikern J. J. Thomson som 1897 (när!) observerade det första katodstråleröret till T. B. Angerer (vem!) som utforskade cancer lipid-metabolism; jämför olika kemiska avbildningstekniker och deras förmåga att svara på frågorna vad? och var?; och skildrar en doktorands försök till att bidra, inte bara igenom att förbättra ToF-SIMS-tekniken, till de stor frågorna som att bota sjukdom, stoppa miljöförstöring och göra framsteg inom vetenskapen. Om jag verkligen har bidragit kan bara tiden utvisa.

Nu vet vi om vad, var, hur, när, vem, men VARFÖR? ... det lämnar vi bäst till filosoferna.

III. List of Publications

I. **3D Imaging of TiO_2 nanoparticle accumulation in *Tetrahymena* pyriformis.**
T. B. Angerer, J. S. Fletcher
Surf. Interface Anal. 46, 198-203 (2014).[1]

II. **High energy gas cluster ions for organic and biological analysis by time-of-flight secondary ion mass spectrometry.**
T. B. Angerer, P. Blenkinsopp, J. S. Fletcher
Int. J. Mass. Spectrom. 377, 591-598 (2015).[2]

III. **Measuring Compositions in Organic Depth Profiling: Results from a VAMAS Interlaboratory Study.**
Alexander G. Shard, Rasmus Havelund, Steve J. Spencer, Ian S. Gilmore, Morgan R. Alexander, Tina B. Angerer, Satoka Aoyagi, Jean-Paul Barnes, Anass Benayad, Andrzej Bernasik, Giacomo Ceccone, Jonathan D. P. Counsell, Christopher Deeks, John S. Fletcher, Daniel J. Graham, Christian Heuser, Tae Geol Lee, Camille Marie, Mateusz M. Marzec, Gautam Mishra, Derk Rading, Olivier Renault, David J. Scurr, Hyun Kyong Shon, Valentina Spampinato, Hua Tian, Fuyi Wang, Nicholas Winograd, Kui Wu, Andreas Wucher, Yufan Zhou, and Zihua Zhu
J. Phys. Chem. B **119**, 10784-10797 (2015).[3]

IV. **Improved Molecular Imaging in Rodent Brain with Time-of-Flight-Secondary Ion Mass Spectrometry Using Gas Cluster Ion Beams and Reactive Vapor Exposure.**
T. B. Angerer, M. D. Pour, P. Malmberg, J. S. Fletcher,
Anal. Chem. 87, 4305-4313 (2015).[4]

V. **Optimizing sample preparation for anatomical determination in the hippocampus of rodent brain by ToF-SIMS analysis.**
T. B. Angerer, A. S. Mohammadi, J. S. Fletcher,
Biointerphases 11, 02A319 (2016).[5]

VI. **Lipid Heterogeneity Resulting from Fatty Acid Processing in the Human Breast Cancer Microenvironment Identified by GCIB-ToF-SIMS Imaging**
T. B. Angerer, Y. Magnusson, G. Landberg, J. S. Fletcher
Anal. Chem. 88, 11946-11954 (2016).[6]

IV. Contribution Report

I. I was responsible for cell cultures, sample preparation, conducting the experiments, optimising the analysis conditions, performing the ToF-SIMS analysis, data treatment, data analysis interpretation and generating of figures, writing the majority manuscript and responding to reviewer comments.

II. I assisted in optimising the analysis conditions; I performed the ToF-SIMS analysis on Irganox, I was responsible for data treatment, data analysis, the interpretation and generating of figures for brain samples and Irganox; I wrote parts of the manuscript and responded to reviewer comments.

III. I assisted with optimising the analysis conditions for the 40 keV GCIB experiments, analysed the samples and generated depth profiles, calculated the layer compositions and reported the results to the National Physical Laboratory (NPL, UK).

IV. I assisted with sample preparation; I conducted the majority of the experiments, optimised the analysis conditions, performed the ToF-SIMS analysis, data treatment, data analysis and interpretation, generated most of the figures, wrote parts manuscript and responded to reviewer comments.

V. I assisted with sample preparation; I conducted the majority of the experiments, optimised the analysis conditions, performed the ToF-SIMS analysis, data treatment, data analysis and interpretation, generated most of the figures, wrote the majority manuscript and responded to reviewer comments.

VI. I assisted with sample preparation; I conducted the ToF-SIMS analysis and optimised the analysis conditions, was responsible for data treatment, data analysis and interpretation, generated the figures, wrote the manuscript and responded to reviewer comments.

V. Publications not included in the Thesis

(S) I. **Maximising the potential for bacterial phenotyping using time-of-flight secondary ion mass spectrometry with multivariate analysis and Tandem Mass Spectrometry.**
Patrick M. Wehrli, Erika Lindberg, Tina B. Angerer, Agnes E. Wold, Johan Gottfries, John S. Fletcher
Surf. Interface Anal. **46**, 173-176 (2014).[7]

(S) II. **Analysis of liposome model systems by time-of-flight secondary ion mass spectrometry.**
Jelena Lovrić, Jacqueline D. Keighron, Tina B. Angerer, Xianchan Li, Per Malmberg, John S. Fletcher, Andrew G. Ewing
Surf. Interface Anal. **46**, 74-78 (2014).[8]

(S) III. **Significant Enhancement of Negative Secondary Ion Yields by Cluster Ion Bombardment Combined with Cesium Flooding.**
Patrick Philipp, Tina B. Angerer, Sanna Sämfors, Paul Blenkinsopp, John S. Fletcher, and Tom Wirtz
Anal. Chem. **87**, 10025-10032 (2015).[9]

(S) IV. **Cholesterol Alters the Dynamics of Release in Protein Independent Cell Models for Exocytosis.**
Neda Najafinobar, Lisa J. Mellander, Michael E. Kurczy, Johan Dunevall, Tina B. Angerer, John S. Fletcher, and Ann-Sofie Cans
Sci. Rep.-Uk **6**, (2016).[10]

(S) V. **Investigating the Role of the Stringent Response in Lipid Modifications during the Stationary Phase in E. coli by Direct Analysis with Time-of-Flight-Secondary Ion Mass Spectrometry**
P. M. Wehrli, T. B. Angerer, A. Farewell, J. S. Fletcher, J. Gottfries
Anal. Chem. **88**, 8680-8688 (2016).[11]

Table of Contents

Chapter I: Introduction

1 Scope

The aim of this project was to broaden the range of samples that can be analysed using imaging time-of-flight secondary ion mass spectrometry (ToF-SIMS) with focus on biological/organic materials and to generate new knowledge from these of samples, as well taking a critical look on past research and the validity of results using standard techniques.

2 Lipids

Lipid is a term that summarises a large, highly diverse group of naturally occurring molecules that include fats, waxes, sterols, fat-soluble vitamins (such as vitamins A, D, E, and K), mono-, di- and tri-O-acylglycerol (IUPAC term, other names are more commonly used *e.g.* triglyceride) and phospholipids. They occur in all living organisms as well as everywhere in the human body. The main biological functions of lipids include storing energy, signalling, and acting as structural components of cell membranes. 50% of most animal cell membranes are lipid, assembled in a lipid-bilayer; nearly all of the remainder is protein. A 1 μm × 1 μm area of lipid bilayer contains approximately 5×10^6 lipid molecules and about 10^9 lipid molecules cover a whole (small) animal cell. All lipid molecules in cell membranes are amphipathic (or amphiphilic)—that is, they have a hydrophilic or polar head and hydrophobic or nonpolar tails.[12]

LIPID MAPS® is an online database established with the goals to classify lipids, understand

Category	Abbreviation	Structures in Database
Fatty acyls	FA	2678
Glycerolipids	GL	3009
Glycerophospholipids	GP	1970
Sphingolipids	SP	620
Sterol Lipids	ST	1744
Prenol Lipids	PR	610
Saccharolipids	SL	11
Polyketides	PK	132

Table 2-1 Lipid categories, abbreviations and number of structures found in the database as established by LIPID MAPS.

their metabolism and involvement in disease and make this data available to the scientific community to facilitate development of more effective disease treatments.[13] The lipid maps classification system is the first internationally accepted lipid classification, nomenclature, and structural representation system which puts lipids into 8 categories, as shown in Table 2-1.

For studies of mammalian cells/organisms the focus lies on glycerolipids (mainly storage fats), glycerophospholipids and sphingolipids (both of which are major structural components of biological membranes and take part in signalling). Molecules within those groups have similar structures but are mainly distinguished by different head-groups and fatty acyls "tails".

2.1 Lipid Synthesis

Pyruvate, the conjugated base to pyruvic acid ($C_3H_4O_3$) is the simplest of the alpha-keto acids, with a carboxylic acid and a ketone functional group. Pyruvate is a key element in several metabolic pathways. It can be generated from carbohydrates (*e.g.* glucose) and fats *via* the glycolytic pathway and β-oxidation and is either resynthesised to glucose *via* gluconeogenesis or used as building block for *e.g.* amino acids. Through interactions with the pyruvate dehydrogenase complex (PDC) pyruvate is converted into acetyl-CoA. In animals this step is irreversible and commits the pyruvate molecule to one of two fates. Acetyl-CoA can be fed into the citric acid cycle where it is further oxidised to CO_2, with the concomitant generation of energy. Alternatively, when energy is readily available (high adenosine triphosphate, ATP) it can be used to synthesize fatty acids through carboxylation by acetyl-CoA carboxylase into malonyl-CoA, the first committed step in the synthesis of fatty acids (*de novo* fatty acid synthesis). From those primary molecules, through a series of elongation and desaturation events, different fatty acids are generated with carbon chains containing 4-30 carbon atoms and up to 6 double bonds (3 if the fatty acid was synthesised *de novo* in mammalian cells). In mammals this conversion occurs primarily in the liver where the fatty acids are combined with glycerol to form diacylglycerides and triacylglycerides (DAGs and TAGs, **glycerolipid** species). TAGs in adipose tissue are the major energy reservoir for most mammals during starvation periods. Apart from energy storage, 2 fatty acid chains can also be combined with a head-group to form different classes of **glycerophospholipids**, or through a reaction with serine, be converted into **sphingolipids**. Alternatively fatty acids from the diet can be used to generate lipids (the main source of fatty acids for lipids).[14]

Through the condensation of acetyl-CoA with acetoacetyl-CoA (and additional steps) cholesterol is generated. Cholesterol plays an important role as a structural component of cellular membranes but it can also be used to synthesize the steroid hormones, bile salts, and vitamin D (**sterol lipids**).[14]

β-oxidation is in essence the reverse of those processes, the catabolic process by which fatty acid molecules are broken down in the mitochondria to generate acetyl-CoA.[14]

2.2 Lipid Classes and Functions

This section does not contain all lipid species and classes but focusses on the ones that are often observed with ToF-SIMS and are highly abundant in the samples included in this thesis.

2.2.1 Fatty Acids

A fatty acid is a carboxylic acid with a long saturated or unsaturated aliphatic chain. Since they are being generated *via* 2 carbon Acetyl-CoA molecule extensions most naturally occurring fatty acids have an unbranched chain with an even number of carbon atoms (4-30). Odd-chained and branched fatty acids can occur for example in protozoa and bacteria, where they make up to 16.5% of bacterial fatty acids.[15] Fatty acids can be in circulation as free fatty acids (FFA) or bound in lipids as membrane constituents, DAGs, and TAGs. Fatty acid chain length and saturation status can have influence on membrane fluidity.[14]

2.2.1.1 Nomenclature

The most common fatty acids have trivial names (*e.g.* Linoleic acid) which have the advantage that they are memorable and refer to only one specific FA species, but they provide no information about the structure of the molecule. Fatty acids are categorised in a number of ways: **Chain length**: short-chain fatty acids (SCFA) with fewer than six carbons, medium-chain fatty acids (MCFA) with 6–12 carbon atoms, long-chain fatty acids (LCFA) with 13 to 21 carbon atoms (*e.g.* LCFA, linoleic acid, C18:2 →18 carbon atoms) and very long chain fatty acids (VLCFA) with more than 22 carbons; **Saturation**: saturated fatty acids (SFA), mono-unsaturated fatty acids (MUFA) and poly-unsaturated fatty acids (PUFA, linoleic acid, C18:2 → 2 unsaturated double bonds) ; **Double bond conformation**: cis-fatty acids (also indicated with Z) where the two hydrogen atoms adjacent to the double bond face the same way (common in nature, linoleic acid has 2 double bonds in cis conformation: cis-cis-18:2, (9Z, 12Z)18:2) or

trans-fatty acids (indicated with E) where they face opposite ways (mainly found in processed foods)[16]; **Double bond position and availability**: the position of the (first) double bond (x) can be noted counting from the carboxy- (C-x or Δ^x , *e.g.* 18:2$\Delta^{9,12}$) or, more commonly used, from the methyl-end (ω-x or n-x, *e.g.* 18:2$_{\omega 6}$) of the fatty acid chain. Mammals lack the enzyme capable of producing ω3 and ω6 fatty acids, therefore those FAs are considered *essential*, while saturated FAs, ω7 and ω9 FAs are non-essential.[17] For example linoleic acid is an essential fatty acid produced by plant cells that cannot be synthesised in mammalian cells from other carbon sources.

Together this results in multiple ways to specify a certain fatty acid. For example linoleic acid can be written down as: (9Z,12Z)-octadeca-9,12-dienoic acid (IUPAC name), cis-C18:2ω6 and many other variants that can all be found in the literature. In mass spectra generated using ToF-SIMS cis and trans double bonds cannot be distinguish nor is it possible to know the position of the double bond without further analysis since those differences do not change the mass of the molecule. The carbon number and number of double bonds can be determined. Therefor it is common to refer to linoleic acid simply as C18:2 or FA(18:2).

2.2.2 Glycerophospholipids

A glycerophospholipid is a molecule most commonly containing 2 fatty acid tails, the nonpolar part of the lipid, connected *via* a glycerol linker to a phosphate and a polar head-group. According to IUPAC, it is any derivative of glycerophosphoric acid that contains at least one O-acyl, or O-alkyl, or O-(1-alkenyl) group attached to the glycerol residue.[18] The different head-groups are responsible for the different functions those lipids. The lipid membrane composition of a typical nucleated mammalian cell is listed in Table 2-2.[19] The molecular structure of glycerophospholipids, the different head groups and net charges at pH 7 are displayed in Figure 2-1.[20] Most are detected as $[M-H]^-$ in negative ion mode ToF-SIMS.

Lipid	% Total lipids
Phosphatidylcholine	45–55
Phosphatidylethanolamine	15–25
Phosphatidylinositol	10–15
Phosphatidylserine	2–10
Phosphatidic acid	1–2
Sphingomyelin	5–10
Cardiolipin	2–5
Glycosphingolipids	2–5
Cholesterol	10–20

Table 2-2 Average lipid composition as percentage of the total lipid content of a typical, nucleated, mammalian cell membrane.[19]

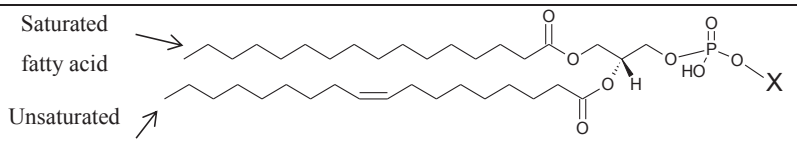

Glycerophospholipid (= R, general structure)

Name of glycerophospholipid	Name of X	Formula of X	Net charge (at pH 7)
Phosphatidic acid	-	R – H	-1
Phosphatidylethanolamine	Ethanolamine	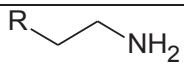	0
Phosphatidylcholine	Choline	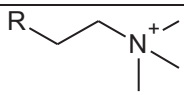	0
Phosphatidylserine	Serine	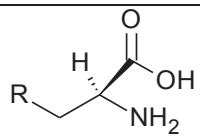	-1
Phosphatidylglycerol	Glycerol	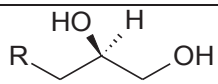	-1
Phosphatidylinositol 4,5-bisphosphate	Myo-Inositol 4,5-bisphosphate	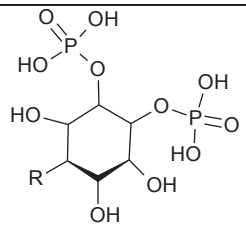	-4
Cardiolipin R_1/R_2 = fatty acids	Phosphatidylglycerol	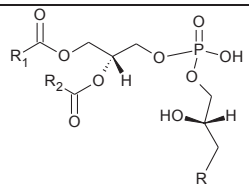	-2

Figure 2-1 Glycerophospholipids: Diacylglycerol linked to head-group alcohols through a phosphodiester bond. Phosphatidic acid, a phosphomonoester, is the parent compound. Each derivative is named for the head-group alcohol (X), with the prefix "phosphatidyl-." In cardiolipin, two phosphatidic acids share a single glycerol.[20]

2.2.2.1 Phosphatic Acid (PA)

Phosphatic acid (PA) is the most simple of the glycerophospholipids since its head-group is only a hydrogen atom. It mainly is the precursor molecule for all other glycerophospholipids. PA is converted into DAGs, TAGs and phosphatidylinositol (PI), phosphatidylglycerol (PG), phosphatidylserine (PS) *via* the CDP-DAG pathway (cytidine diphosphate diacylglycerol) or the Kennedy pathway. In the liver phosphatidylethanolamine (PE) and phosphatidylcholine (PC) can be generated from PS but those species can also be synthesised from DAGs.[21-22] Apart from its precursor function it plays a role in vesicle formation and other cellular events that require a highly curved cell membrane (*e.g.* membrane fusion) because of its stearic properties (small head, big fatty acid tails).[23]

2.2.2.2 Phosphatidylglycerol (PG)

Phosphatidylglycerol (PG) is the second most abundant lipid species in bacterial cell membranes and it can be used as a precursor for cardiolipins. PG is found in mammalian cells as well but in low abundance. The only exception is the lung surfactant where it can be the second most abundant phospholipid.[24]

2.2.2.3 Phosphatidylinositol (PI)

Phosphatidylinositols (PI) are important lipids in all eukaryotes as both, structural components of the cell membrane and as signalling molecules. The synthesis of PIs is mediated by the CDP-DAG pathway but takes a different route from the branch that leads to PE and PC. PIs are mostly present in the brain but occur in all tissues and the most abundant species is PI(18:0/20:4).[25] PI is used to synthesise inositol polyphosphates (IPs), other complex sphingolipids, and phosphoinositides (PIPs), which vary in the number and arrangement of additional phosphate residues attached to one or more of the six carbons in the inositol ring on its head-group (Figure 2-1). PI and its metabolites regulate a diverse set of cellular processes such as glycolipid anchoring of proteins (due to its negative charge),[26] signal transduction,[27] mRNA export from the nucleus,[28] vesicle trafficking,[29] and serve as reservoirs of secondary messengers.[30] They play an important role in cancer as they are involved in cell growth and proliferation.[31] Due to the multiple -OH groups on its head-group the probability for PI to carry a negative charge is high which makes it amenable for ToF-SIMS (detected as $[M-H]^-$).

2.2.2.4 Phosphatidylethanolamine (PE)

An important building block to generate phosphatidylethanolamine (PE) is ethanolamine. While plants and algae can synthesise ethanolamine *de-novo* from serine, mammals cannot and have to acquire it through their diet. Alternatively PE can be synthesised from PS *via* decarboxylation. 70–80% of total phospholipids in *E. coli* are PE[32] and in eukaryotic cells it is the second most abundant lipid class after PC.[33] Due to its rather small head-group it has a conical shape which introduces curvature stress to the membrane, therefore it is mostly found on the inner side of the lipid-bilayer. Similar to PA, its shape makes it important for cell division, membrane fusion and fission events.[34] PE is a zwitterionic molecule which makes it possible to detect it in positive and negative ion mode with mass spectrometry. This also enables PE to establish hydrogen bonds with a wide variety of amino acid residues and due to its charge distribution it can keep transmembrane domains of membrane proteins in place.[35] When it comes to cell signalling, PE mainly serves as precursor to biologically active molecules. (*e.g.* DAGs, FAs, and PA generated from PE metabolism can act as secondary messengers).[36]

2.2.2.5 Phosphatidylserine (PS)

Phosphatidylserine (PS) is a lipid that is actively held in the inner cell membrane by the enzyme flippase.[37] PS is only exposed due to damage or death. When a cell undergoes apoptosis PS is transported to the outer cell membrane where it functions as a signalling molecule for macrophages.[38] PS also promotes blood coagulation.[39]

2.2.2.6 Phosphatidylcholine (PC)

Phosphatidylcholine (PC) is the most abundant lipid species and it dominates the outer leaflet of the lipid membrane. PC can be degraded and its choline head-group is used to form acetylcholine, a neurotransmitter.[40] Its shape is roughly cylindrical (depending on its fatty acid tails) so it does little to promote membrane curvature. PC can be synthesised *via* the CDP-choline pathway (Kennedy) or *via* methylation of PE.[41] Due to the nitrogen in the choline head-group the molecule is either neutral (in combination with a negatively charged phosphate group) or it can acquire a positive charge.

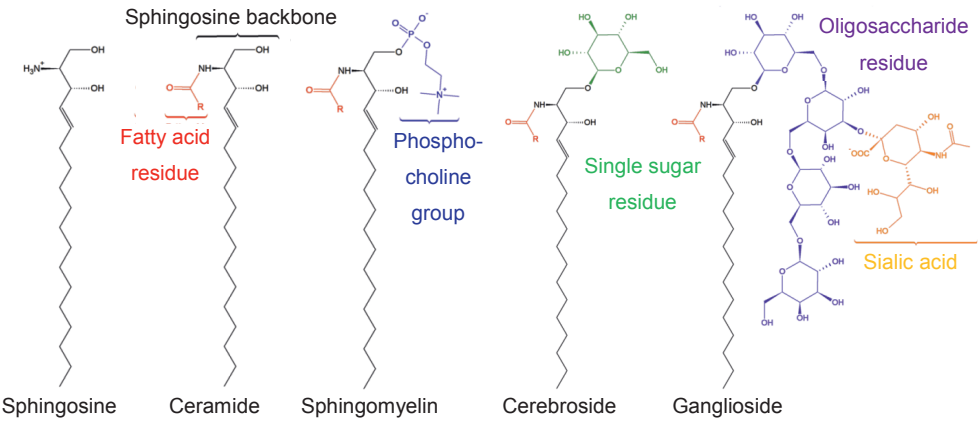

Figure 2-2 Molecular structure of different sphingolipids, R = different fatty acids. Adapted; Licence: CC-BY-3.0[42]

2.2.3 Sphingolipids

Different to glycerophospholipids (2 fatty acid tails, attached *via* ester bonds to glycerol + phosphate and different head-groups) sphingolipids constitute a class of lipids defined by their eighteen carbon amino-alcohol backbones plus 1 fatty acid (=R as shown in Figure 2-2).[42] In contrast to most glycerophospholipids, simple sphingolipids can flip between the inner and outer leaflet of the cell membrane. Sphingosine is the simplest form of this compound. Derivatisation with different acyl-CoA molecules (attaching a fatty acid) forms the class of ceramides, which can serve as a precursor for other lipids. Addition of a phosphocholine head-group forms sphingomyelins, and addition of various sugar molecules forms glycosphingolipids, such as simple cerebrosides (galacto-, glucoceramide) or the large and complex gangliosides.[43]

2.2.3.1 Sphingomyelin (SM)

Sphingomyelins (SM) are the most abundant complex sphingolipids in mammalian cells and are necessary for cell survival in culture (contrary to galacto- and glucoceramides). SMs are present in all cells but especially abundant in myelin sheets around axons (hence the name). Their role as a secondary messenger has only been confirmed to be *via* hydrolysis to form ceramides, which are involved in the apoptosis signalling pathway,[44] and *via* the transfer of the phosphocholine head-group from PC, which produces DAG, another bioactive lipid species. Therefore SM is assumed to be a regulator in cellular fate.[43] Similar to PC it carries no net charge but it can ionise positively $[M+H]^+$ or negatively *via* the loss of a methyl group $[M-CH_3]^-$. In ToF-SIMS

spectra SM can be easily distinguished from PC, as SM has 2 nitrogen atoms and therefore ends up having an uneven mass, PC contains one nitrogen and has an even mass. This is due to the nitrogen rule, nitrogen is special since it has an even mass (14 Da.) but can form an odd number of covalent bonds (3 bonds). Therefore a neutral organic molecule containing only the atoms C, H, O, N, S, P, or any halogen has an odd nominal mass if it contains an odd number of nitrogen atoms and vice versa for even numbers.[45] This is inverted for ToF-SIMS due to the addition of $[M+H]^+$ (*m/z* 1), $[M+Na]^+$ (*m/z* 23) or $[M+K]^+$ (*m/z* 39)) to ionise the molecule in positive ion mode.

2.2.3.2 Sulfatide (ST)

Sulfatides (ST) are produced from galactosylceramide *via* the enzyme galactosylceramide sulfotransferase. About 4% of all lipids in myelin sheath are sulfatides[46] and studies on mice models deficient in this enzyme indicate that many myelination defects may be due to a lack of sulfatide production.[47] Sulfatide is a multifunctional molecule involved in various biological processes, not only in the nervous system but also in insulin secretion, the immune system, cancer, haemostasis/thrombosis, bacterial and viral infections.[48] The sulphate included in the head-group gives the lipid acidic properties, therefore it can be found in negative ion mode mass spectra as $[M-H]^-$ species.

2.2.3.3 Gangliosides

Gangliosides are a diverse group of lipids composed of a complex glycosphingolipid with one or more sialic acids (*e.g.* n-acetylneuraminic acid, NANA) linked to a sugar chain. They are most abundant in the nervous system and so far 188 species have been identified. They are mainly located in the outer cell membrane leaflet. Due to the large head-group reaching far beyond the cell membrane they are involved in cell-cell recognition, adhesion and signal transduction within specific cell surface microdomains, so called calveole.[49] They undergo multiple changes during brain development, for example in developing brains more simple gangliosides such as GM3 and GD3 are dominant while in the adult brain production is shifted towards complex gangliosides such as GM1 (most abundant species), GD1a, GD1b and GT1b.[50] Due to their acidic nature gangliosides can detected in negative ion mode mass spectra.

2.2.4 Cholesterol

Cholesterol is an essential structural component of animal cell membranes and is required to maintain both, the membranes structural integrity and fluidity. Although mammalian lipid membranes contain an estimated 2000 different lipid species, 30-50 mol % of the membranes is cholesterol. The incorporation of cholesterol makes cell membranes sustainable without cell walls. Essentially it allows animals to move, in contrast to bacteria and plants.[51] Cholesterol can move between the inner and outer leaflet of the membrane and is thought to be able to rapidly react to environmental changes. Cholesterol can serve as precursor of hormones and can regulate incorporation of membrane proteins by adjusting fluidity. Due to its low solubility in water it is transported in the blood stream *via* lipoproteins.[52] For many years it was thought that cholesterol is enriched within so called lipid rafts together with sphingolipids but it has been shown that while sphingolipids are found in domains in the cell membrane, cholesterol is evenly distributed.[53] Cholesterol can be detected in positive mass spectra as $[M+H-H_2O]^+$ and $[M-H]^+$ species and in negative mass spectra as $[M-H]^-$ species although in lower intensities.

3 Mass Spectrometry

Fundamentally, a mass spectrometer is used to measure the mass-to-charge ratios (*m/z*) of ions, a metric from which molecular weight can be determined. This process involves three steps. First, molecules have to be converted to gas-phase ions, a challenging process for molecules in a solid or liquid phase. Next, those ions have to be separated by their *m/z* values in a so called mass analyser. Finally, the separated ions and the abundance of each species with a particular *m/z* value are detected.

Nowadays we experience a constant stream of impressive and important advances in biological mass spectrometry and for each of the previously mentioned steps a large variety of techniques and instrumentation are available. Adjusted to answer almost any question a scientist might have, mass spectrometry has enabled significant discoveries and clinical developments in the last 2-3 decades (*e.g.* tandem mass spectrometry disease testing).[54] This can lead to the impression that the technology is a recent innovation but in fact, mass spectrometry has had a long and interesting history and it has played a central role in many important scientific advances since 1900.

3.1 A Brief History of Mass Spectrometry

This section mainly covers the significant inventions/discoveries leading to the development of imaging ToF-SIMS, along with other important events in mass spectrometry history.[55]

3.1.1 Cathode Rays

The first step to make mass spectrometry possible can be attributed physicist J. J. Thomson. By using an electric field inside a cathode ray tube he discovered the electron in 1897 (Nobel Prize in Physics 1906). This led him to the development of a crude 'mass spectrograph' (then called a parabola spectrograph) to measure the atomic weights of elements.[56] In this instrument, ions generated in discharge tubes were passed into electric and magnetic fields, which made the ions move through parabolic trajectories. The resulting rays were detected on a fluorescent screen or photographic plate. Further improvements of his device were made by Thomson's students who designed a mass spectrometer in which ions were dispersed by mass and focused by velocity. This increased the mass resolution by an order of magnitude and enabled one of them, F.W. Aston to discover ^{20}Ne and ^{22}Ne which proved the existence of stable isotopes and gained him the Nobel Prize in Chemistry1922.[57]

3.1.2 First Industrial Use

With the development of magnetic sector instruments in the 1940s MS did become of public interest for the first time. Professor Alfred O. C. Nier designed and built several revolutionary instruments which allowed more sensitive and precise measurements of isotopes and their ratios, including the 60° sector field instrument, which greatly reduced the size and power consumption of the magnet and the so called Nier-Johnson mass spectrometer, which combines electrostatic and magnetic analysers in a unique conformation. Nier's inventions were used in the Manhattan project to purify and assess the enrichment of the fissionable isotope of uranium, ^{235}U.[58] The Calutron, a three-story-high version of Nier's sector instrument, separated ^{235}U for the first atomic bomb. Nier also contributed to biology/medicine. He discovered the ^{13}C isotope and subsequently purified the isotope for use in tracer experiments to understand metabolic pathways.[59] After the 2nd world war, prompted by the petroleum industry, further development resulted in double-focusing magnetic sector instruments that used an electric sector to correct for kinetic energy spread in ions before separation in the magnetic field and ushered in high-resolution mass spectrometry. Although this led to even better mass accuracy and peak capacity

the drawback of those instruments was that they were quite expensive. The cheaper time-of-flight (ToF), quadrupole, and ion trap mass spectrometers were developed in parallel.

3.1.3 Time-of-Flight Mass Analyser

In 1946 William E. Stephens proposed the concept of a time-of-flight (ToF) mass spectrometer.[60] The principle of a ToF analyser is that ions are separated by differences in their velocities. As they move in a straight path towards a collector they arrive in order of increasing mass-to-charge ratio. The advantages of this analyser are that it is fast, it is applicable to chromatographic detection, and it can be used for the analysis of large biomolecules, among other applications. Bendix Corporation was the first to commercialise ToF mass spectrometers but in the beginning mass resolution was poor, lagging far behind even the most simple magnetic sector instruments at the time. A real game changer was the invention of the reflectron by Boris A. Mamyrin in 1973/4 which corrects for the effects of the kinetic energy distribution of the ions as well as doubling the length of the flight tube and therefore achieving a better separation of the masses.[61] With this improvement ToF-analysers were able to match the performance of sophisticated, double-focusing mass spectrometers for only a fraction of the cost.

On a side note, the highest currently available broadband mass resolving power ($m/\Delta m$ = 100,000) and mass accuracy (<1 ppm) can be achieved with Fourier transform ion cyclotron resonance mass spectrometry (FT-ICR MS) which was also invented in 1974 by Melvin B. Comisarow and Alan G. Marshall.[62]

3.1.4 Secondary Ion Mass Spectrometry

Secondary ion mass spectrometry (SIMS) was the first desorption technique to greatly advance the capabilities of MS. It is a technique in which a beam of ions is used to ionise molecules on a surface. Richard E. Honig established SIMS as an analytical method in the 1950s.[63]

At the beginning SIMS was mainly considered a new technique for elemental analysis of solid materials with sputtering being an efficient and universal way for ionisation. Due to a lack of sensitivity, the first SIMS instruments operated in the “dynamic” mode with high primary ion currents, eroding several 100 monolayers in one analysis. SIMS could only be applied for bulk characterisation of solids. This changed when Alfred Benninghoven and co-workers at the University of Cologne and later Münster proposed *static* SIMS where only about 1% of the surface layer was impacted by the analysis beam. Although in static SIMS the surface stays

largely untouched, sufficient signals could still be detected due to further developed SIMS instrumentation and more sensitive detectors, capable of single ion counting (electron multiplier).[64]

3.1.5 Bio-Molecules

From the late 1950s and into the early 1960s, Klaus Biemann led efforts to use mass spectrometry to measure the molecular weight of small molecules and biomolecules to verify their structure. The technology used by Biemann, electron impact ionisation (EI), created fragment ions by using a beam of energetic electrons to bombard volatilised molecules. Making biomolecules, which are often polar and charged, compatible with mass spectrometry was a challenge. By derivitising free amino groups and carboxylic acids in peptides to reduce polarity and charge, sufficient volatility could be created to acquire a mass spectrum of short peptides (two to three amino acids).[65]

Further improvement offered the development of chemical ionisation methods (CI) developed by Munson & Field,[66] where first a gas is ionised using EI and those charges are then transferred as a result of ion-molecule reactions. This ionisation method causes much less fragmentation, so larger molecules could be analysed.

One big issue at this time was that the analysis of large organic compounds required them to be in gas-phase, so they needed to be volatile and/or be exposed to heat to be evaporated. For non-volatile, unstable molecules those conditions were problematic. SIMS could offer a solution but the first SIMS instruments were lacking sensitivity and mass range. To overcome those issues new instrumentation and/or protocols were needed. Due to the challenges in sample treatment, one development was the invention of fast atom bombardment (FAB) by Michael Barber, Bob Bordoli and co-workers, also called liquid-SIMS where beams of neutral atoms are used to ionise compounds gently from a glycerol surface. The glycerol and sample molecules are sputtered into the gas phase, making it possible to obtain spectra of large, non-volatile organic molecules.[67] Then in 1985 Michael Karas and Franz Hilllenkamp developed matrix-assisted laser desorption ionisation (MALDI).[68] Similar to FAB, MALDI uses a matrix to ionise the sample molecules but rather than being bombarded by fast particles, samples are ‘bombarded’ by photons from a UV-light laser. Its unique capability to ionise very large proteins, carbohydrates and even DNA

as singly charged ions, allowed accurate mass measurement of large molecules that were never possible before.

A different development was to further improve SIMS instrumentation by, for example, coupling it to a ToF analyser, which enabled the combination of the fast analysis speed of SIMS with a theoretically unlimited mass range. In 1983 Benninghoven *et al.* built the first commercially available, high performance time-of-flight-secondary ion mass spectrometer, the ToF-SIMS I and the development is still going on to this day.[69] The early ToF-SIMS instruments used single atom* primary ion beams (*e.g.* $*O_2^+$, O^-, Cs^+, Ga^+, Xe^+ and Ar^+) which caused high sub surface damage, fragmented bigger molecules and produced only small useful secondary ion yields. At that time SIMS was not well suited for the analysis of organic compounds. The introduction of cluster primary ions like Au_3^+,[70] Bi_3^+,[71] SF_5^+,[72] and C_{60}^+[73-74] showed huge improvements concerning higher mass ion yield. In particular C_{60}^+ also had the advantage of greatly reduced subsurface damage.[75] C_{60}^+ allowed SIMS analysis to go beyond the static limit, back to a dynamic SIMS mode but contrary to before, while still generating intact molecular information, removing only a few monolayers in one analysis and keeping the underlying layers intact. This meant that inorganic and organic compounds could be studied in depth, so one and the same surface could be analysed multiple times. While eroding the sample, subsurface molecular information was gained.[76-79] Now the trend goes towards gas cluster ion beams (GCIB) and primary ions with ever increasing size, like big argon clusters (Ar_{500}^+ - Ar_{4000}^+ and more).[80-82] This brings the capabilities of SIMS imaging closer to the MALDI regime, since intact molecules with sizes of several kDa. can be ionised and sputtered off a sample.[83]

3.1.6 Mass Spectrometric Imaging

By generating spectra from specific points on a sample surface, often using a focused ion beam or laser to ablate material, a “chemical map” of the sample surface is generated. This is called mass spectrometric imaging. SIMS is particularly well suited for imaging because of the ability to focus the ion beam and the broad range of secondary ions generated. SIMS is not the only mass spectrometry technique capable of imaging but it was the first. Theoretically invented in 1949[84] by Herzog and Viehbock of Vienna University the first SIMS device capable of imaging was completed by Liebel and Herzog in 1961, and it was used for the surface analysis of metals. To this day SIMS is mainly used for inorganic analysis (*e.g.* semiconductors). The first SIMS

images were published in 1962 by a French research team.[85] Spatial resolution in SIMS images was comparable to that of a light microscope with a device presented by Liebel in 1967 that could achieve a spatial resolution of 1-1.5 µm, however, at first those SIMS instruments were not suitable for analyses of biological macromolecules.[86]

The utilisation of cluster ions such as $C_{60}^{+}$and argon gas clusters as primary ion sources are beginning to change that. The first MALDI imaging publication was presented by Caprioli *et al.* in 1997.[87] Although lacking the capabilities of SIMS concerning spatial resolution, MALDI can provide information based on peptide and intact protein signal from tissue slides.

Newer developments go towards MS-imaging in ambient conditions. This can be done with desorption electrospray ionisation (DESI) and was first shown in 2004 by Cooks *et al*[88] and very recently location specific mass spectrometry has managed the leap into the operating theatre with the invention of the iKnife in 2013 by Takáts *et al*.,[89] a scalpel that feeds back information to the surgeon about the malignant state of the tissue in real time during surgery.

The technical details of those methods will be covered in section 3.3 Comparison of Various Analysis and Imaging Techniques.

3.2 ToF–SIMS Technique

Time-of-flight – secondary ion mass spectrometry (ToF-SIMS) is an analytical method that uses a focused, (and for the majority of ToF-SIMS instruments also pulsed) energetic particle beam, or so called primary ions, to sputter chemical species from a surface. The primary ions can consist of atomic, small or large clusters or polyatomic ions (Ar^{+}, Ga^{+}, Cs^{+}, O_2^{+}, Au_3^{+}, Bi_3^{+}, SF_5^{+}, C_{60}^{+}, Ar_{4000}^{+}) which, on impact at the sample surface, eject electrons, atoms, molecules and fragments thereof. Ejected species produced closer to the site of impact tend to be dissociated ions and those generated farther from the impact site tend to be molecular compounds. Depending on the nature of the primary ion more or less atoms and fragments *vs.* intact molecular species are ejected. The vast majority (about 99%) of ejected species are neutral and therefore not useful for the analysis but a small portion are charged or become ionised (with varying ionisation probabilities for each species) and come off the sample as so called secondary positive or negative ions. The charged species can be extracted, then redirected and accelerated into a ToF mass analyser. Inside the ToF on the flight path towards a detector the secondary ions

are separated according to their mass to charge ratio, with “heavier” species flying slower than “lighter” ones. Depending on the instrumental setup a ToF-analyser can produce mass spectra with a mass accuracy of 5 ppm, a mass resolution of typically m/Δm = 10 - 20,000 (some instruments up to 80,000)[90] and theoretically no upper mass limit. However, on conventional ToF-SIMS instruments the mass range is limited to the size of molecules that are ejected by the ion beam and the mass accuracy generally obtained has been found to be approximately 150 ppm.[91]

3.2.1 Imaging ToF-SIMS

The primary ion beam can be focused and rastered over a sample surface where for each new pixel an individual mass spectrum is recorded. This way a chemical map of the sample surface is generated. Historically SIMS was a highly destructive method mainly suitable for analysing atomic species. Imaging ToF-SIMS of molecular secondary ions used to be bound to the so called *static limit* since ion bombardment of a surface may result in a drastic change of its chemical composition and structure. These changes include sputtering, amorphisation, implantation, diffusion, chemical reactions, and so on. All these changes are limited to a very small region (the altered surface area is called damage cross section) surrounding the path of the primary ion into the sample. The static limit represents the maximum number of primary ions to analyse only up to 1% (about 10^{13} ions/cm^2 for atomic analysis) of the sample surface so each subsequent primary ion hits an undamaged area. A higher primary ion dose would lead to the analysis of the accumulated damage or changes in the sample from previous impacts, so less molecular information representative for the samples surface chemistry is available.

With the development of bigger primary ion species (C_{60}^+, Ar_n^+) this limitation could be overcome.[92] Those primary ions are either used as analysis beam or just for sputtering to remove damage between analyses. With bigger cluster sizes less damage occurs while sputtering the surface and below. This enables analysis to go beyond the static limit and dynamic SIMS to be performed, where a whole sample layer is removed while sputtering and the sample surface can be analysed multiple times. This way a sample can be analysed not only on the surface but also as a function of depth without losing the entire molecular signal. With a stack of 2D images, 3D models based on molecular information can now be generated using imaging ToF-SIMS.[76, 79, 93-95]

3.2.2 The SIMS Equation

ToF-SIMS can be considered as a qualitative but only semi quantitative method. The ability to generate signal from a single species within a sample depends on a number of parameters and can be summarised using the basic SIMS equation:

$$I_{m^+} = I_p \gamma_m \alpha_m^+ \theta_m \eta_m$$

$\mathbf{I_m}$	secondary ion current/signal of species m
$\mathbf{I_p}$	primary ion flux
$\boldsymbol{\gamma_m}$	sputter yield of species m
$\boldsymbol{\alpha_m^{+/-}}$	ionisation probability in positive/negative ion mode
$\boldsymbol{\theta_m}$	the fractional concentration of m in the surface layer
$\boldsymbol{\eta_m}$	transmission of the analysis system (for species m).

All secondary ions generated in SIMS analysis originate from the topmost layers of the bombarded sample, therefore only the surface concentration $\boldsymbol{\theta_m}$ of analyte m is relevant for the resulting $\mathbf{I_m}$.

$\boldsymbol{\gamma_m}$ and $\boldsymbol{\alpha_m^{+/-}}$ are the two fundamental parameters which can differ greatly between 2 species, leading to variable signal intensities despite being present in the same concentration in the sample surface. Under certain circumstances the signal intensity of one species in one sample is comparable to the intensity of the same species in another sample; therefore ToF-SIMS can be considered as semi-quantitative. This can be complicated due to surface charging and matrix effects. Matrix effect is the altered ionisation rate of an analyte in the presence of other species that can enhance or supress its ionisation. An example is shown in section 6.2.6 Results: Matrix Effects (Paper III). Surface charging is the build-up of positive/negative charges on the surface, slowing down ions of the opposite polarity when leaving the surface, leading to decreased detection of analyte species in the areas of the sample that experience this effect.

3.2.2.1 Ion Flux and Sputter Yield

$\boldsymbol{\gamma_m}$ is the total yield of sputtered particles of analyte m, neutral and ionic, per primary ion impact. It increases linearly with primary ion flux $\mathbf{I_p}$. It also increases with primary ion mass and energy although not linearly. Primary ions can vary from atoms to giant clusters; all with their individual advantages and drawbacks (as stated earlier). $\boldsymbol{\gamma_m}$ tends to maximise with beam energies between

5-50 keV.[96-97] For atomic analysis of pure materials it has been found that sputter yields vary across the periodic table, even when the same primary ion density is used.[98] When analysing organic samples containing large molecules it is important to find the right combination of energy and cluster size to maximize the secondary ion yield for the target molecule. In general with increasing cluster size larger secondary ions can be observed, since the impact can be powerful enough to lift the molecules off the surface (although the primary ions can be deposited on the surface if C_{60} is used below 10 keV)[99] but gentle enough not to fragment those molecules at impact, due to the beam energy being spread over the number of atoms in the cluster. The limiting factor is a threshold in ionisation and sputtering when the energy per atom drops below a certain value (cut-offs between 1 and 5 eV per atom have been reported, depending on the analysed material).[100-101] The maximum beam energy is limited by the instrument and therefore also the maximum useful cluster size. The benefits of using giant gas cluster beams with high energies for organic analysis are currently under investigation (Ar_{4000}^{+}, 40 keV).[2] Even for atomic metal analysis cluster sputtering can be advantageous due to the property of atomic primary ions to penetrate deeply into the surface where the impact energy is absorbed in collision cascades and only a few atoms are being lifted off the surface. Cluster impact is more superficial and the energy is affecting the surface directly as opposed to the collision cascade where energy is deposited below the surface and some returns to the surface leading to ejection. (as suggested by molecular dynamics simulations Figure 3-1).[102]

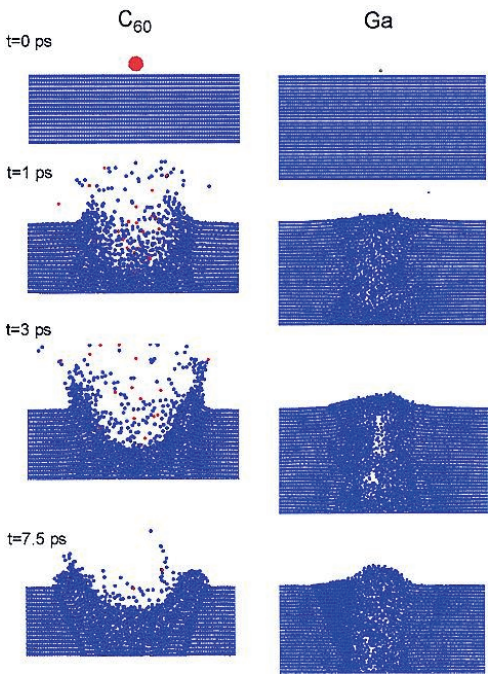

Figure 3-1 Cross sectional view of a collision event leading to ejection of atoms due to 15-keV C60 and Ga bombardment of a Ag{111} surface. Blue, red, and green depict silver, carbon, and Ga atoms, respectively. Reprinted with permission from Z. Postawa, B. Czerwinski, M. Szewczyk, E. J. Smiley, N. Winograd, B. J. Garrison, *Anal. Chem.* 2003, 75, 4402-4407.. Copyright 2003 American Chemical Society.

3.2.2.2 Ionisation Probability

In general the ionisation probability for molecules in SIMS is still poorly understood and requires more research. However there are theories and approximations that help shed light on the highly varying ionisation probabilities for different secondary ion species that can be observed during SIMS experiments.

Ionisation probabilities and ionisation energies for gaseous atoms have been studied in depth and good models are available.[103] For positively charged ions the ionisation energy is defined as the minimum amount of energy required to remove an electron (to infinity) from the atom (X) or molecule in its ground state.[18]

$$X + \text{energy} \rightarrow X^{+} + e^{-}$$

The units for ionisation energy vary from discipline to discipline. In physics, the first ionisation energy is typically specified in electron volts (eV) and refers to the energy required to remove the first electron from a single atom or molecule. In a plot of the ionisation energy against the atomic number some clear trends become visible (Figure 3-2).[103-104]

Two trends are apparent from this data: In general, the first ionisation energy increases as we go from left to right across a row (period) of the periodic table due to the attraction between the nucleus and an electron, which increases with the number of protons in the nucleus (*e.g.* 2nd

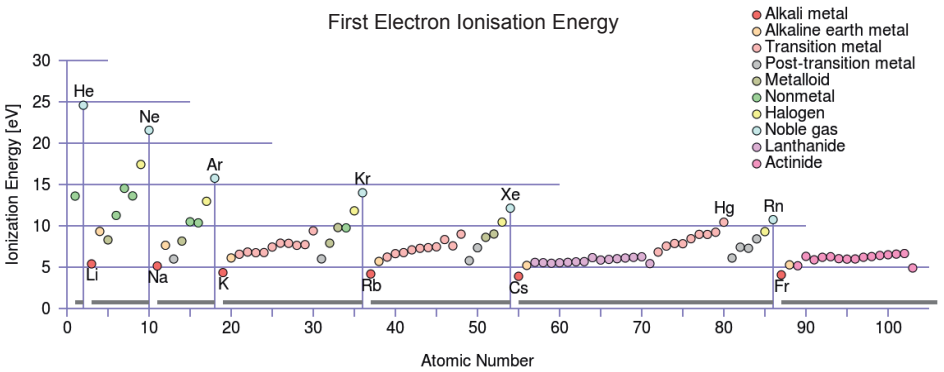

Figure 3-2 Ionisation energy (IE) *vs.* atomic number, trends observed across the periodic tables of elements. Vertical lines separate the periods, elements with the highest/lowest first electron ionisation energy are labelled in each period with their elemental symbols. All elements are colour coded according to the categories listed (*e.g.* Noble Gas), eV values from NIST Atomic Spectra database. Licence: CC-BY-3.0[103-104]

period left-right: Lithium 5.392 eV < Neon 21.564 eV).[103] Moving from the top to the bottom in a column (group) of the periodic table, the electron affinity increases and ionisation energy decreases. The higher electron affinity makes it more likely for an atom to take up one electron and become an anion instead of releasing one (*e.g.* 2nd group top-bottom: Beryllium 9.322 eV > Radium 5.279 eV).[103] Additionally, the principal quantum number of the orbital holding the outermost electron becomes larger further down a column/group of the periodic table which causes the first ionisation energy to decrease. Although the number of protons in the nucleus also becomes larger, the electrons in smaller shells and subshells tend to screen the outermost electrons from the attraction of the positive charges in the nucleus. The likelihood of an atom for becoming a cation or an anion is generally based on the energetically most favourable state of a fully occupied outer electron shell. Nobel gases are already in this favourable state; therefore they require high energies to be ionised.

The nature of the specimen itself will affect the ionisation process; relevant factors here include the chemical and physical properties of the specimen (as previously stated, electronegativity of each atom in the molecule, its ionic or covalent nature, crystal structure, morphology, etc.).[105] When analysing atomic secondary ions the primary ion species itself (significant differences exist in secondary ion yields for metals sputtered with Cs^{+}[106-107]/Ar^{+} ions or O^{-}[108] ions), its energy and flux can effect ionisation. Even if not used as primary ion source, the effect of Cs can be used to increase the ion yield for negative secondary ions (neutral Cs vapour being deposited on the surface during the analysis).[109] Additionally, the ionisation probability depends on the chemical nature of the sample. If a metal surface is oxidised, the ionisation probability of the positive metal ion and the observed yield increases (in general). This increase is not constant for each element. The ionisation probability changes when a reactive primary particle such as O^{-} is used (as mentioned earlier), which leads to an oxidation of the metal atoms in the vicinity of the ion impact and an increase in the ionisation probability.

These measurements work well for free single atoms but ionisation of molecular species with SIMS is complicated by a couple of factors. However one can still find those basic physical properties reflected in SIMS spectra, for example Na^{+} and K^{+} as well as molecules containing those atoms or forming adduct ions with Na^{+}/K^{+}, produce high secondary ion yields in positive ion mode, while molecules containing highly electronegative atoms (halogens, oxygen) are present in negative ion mode spectra.

For analysis of organic samples by SIMS, where molecular ions are generated, the ionisation probabilities of individual compounds are variable and different ionisation mechanisms are possible. The main ion formation process in organic analysis is the formation of pseudo molecular ions *via* protonation $[M+H]^+$ or deprotonation $[M-H]^-$. Other possibilities are: loss of small functional groups (*e.g.*: $[M-CH_3]^+$); molecular radicals M^+, M^-; and cationisation by alkali (*e.g.*: $[M+Na]^+$) or metal addition. Although the ionisation potentials of organic molecules fall within a narrower energy range than those for atoms, the chance that a molecular ion will dissociate/fragment must also be factored into the probability of observing the molecular ion. Fragmentation of large molecules usually leaves the smaller fragment intrinsically charged (m/z <500), while larger fragments are neutral.[97]

For organic analysis, the nature of the primary particle does not have a drastic effect on the ionisation probability. Currently there is no consensus in the scientific community whether or not the impact of the primary ion is contributing to the ionisation probability of molecules, or if only naturally occurring, preformed ions are being sputtered off the surface. It seems that it is the chemical nature of the sample that exerts the dominant effect. In general, organic compounds that exist as preformed ions at the surface, or that can be readily induced to form ions *via* acid/base reactions (resulting in $[M+H]^+$ or $[M-H]^-$ ions) exhibit high ion yields but are always competing for protons with their surrounding molecules. The effect of the surrounding environment on the ionisation probability of a target molecule is called the matrix effect which can enhance or suppress the signal. Organic samples that are more difficult to ionise or that fragment readily do not produce high quality secondary ion mass spectra.

Another factor that complicates predictions for the ionisation efficiency of a specific molecule is due to reactions after desorption, related to gas phase basicity (GPB). GPB, also called absolute or intrinsic basicity of a species,[18] is defined as the negative of the Gibbs free energy change associated with the reaction:

$$M_{(g)} + H^+_{(g)} \rightarrow MH^+_{(g)}$$

GPB values for certain molecules (M) can be quite different from their solution based basicity.[110]

3.2.2.3 Transmission

While most parameters can be adjusted/optimised by the experimenter, transmission is a property of the instrument, largely dependent on its design and cannot be altered by the user without exchanging components. Some instruments allow adjustments that will enhance transmission for some analytes while others are decreased.

3.3 Comparison of Various Analysis and Imaging Techniques

As was touched upon in the history of mass spectrometry, nowadays there are a great variety of analysis and imaging techniques, each with its advantages, disadvantages and variations of the same principal concept (*e.g.* same methods to generate ions coupled with different mass analysers). Here histological/staining techniques, NanoSIMS, ToF-SIMS, MALDI, DESI and chromatography techniques are discussed. This list is by no means extensive, but is meant to represent the range of spatial and/or chemical information one can acquire using modern analysis techniques. The characteristics of some imaging MS techniques are summarised in Table 3-1, reproduced from the imaging mass spectrometry review by von Hove *et al*.[111]

Source	Examples	Environment	Energy	Spot size (d)	Surface current	MW range (*m/z*)
Liquid metal Ion gun	Ga^+, In^+, Au^+ Au^{2+}, Au^{3+}	UHV	>25 eV	>1 µm	1–10 nA	0–3000
Solid-state gun	Cs^+	UHV	10 keV	2–3 µm	<10 nA	0–3000
C_{60}^+ cluster source	C_{60}^+	UHV	5 eV–40 keV	200 nm–200 µm		0–3000
MALDI	Nd:YAG, N_2 Nd:YLF	UHV, HV Ambient	100–200 J/pulse	5–300 µm	n/a	100–500,000
DESI	Solvent (*e.g.* H_2O, MeOH)	Ambient	n/a	>150 µm	0.5–50 nA	100–66,000

Table 3-1 Summary of characteristics and capabilities for different imaging mass spectrometry approaches.[111]

With each technique being constantly developed further, where possible, many of them start to overlap in capabilities (*e.g.* improved spatial resolution with MALDI; the possibility to generate bigger molecular secondary ions with SIMS) but so far one device that can do "it all" has not been developed yet. "It all": within a short analysis time, quantitative signal with 100% true to life, chemical coverage in spectra with infinite mass resolution from images with nanometre spatial resolution. Although it might be possible to build an instrument that could perform all those tasks separately, it would not be very practical and horrendously expensive. Overall, higher mass resolution increases analysis time, bigger analytes require a bigger analysis area, as sensitivity limits resolution and matrix effects also effect sensitivity and quantitation. For now, the only options is to constantly improve sample preparation and instrumentation as well as combining the advantage of different techniques and perform multimodal imaging experiments. A simplified schematic of how different techniques perform with respect to spatial resolution and

chemical information is displayed in Figure 3-3. Each technique is described in the following sections.

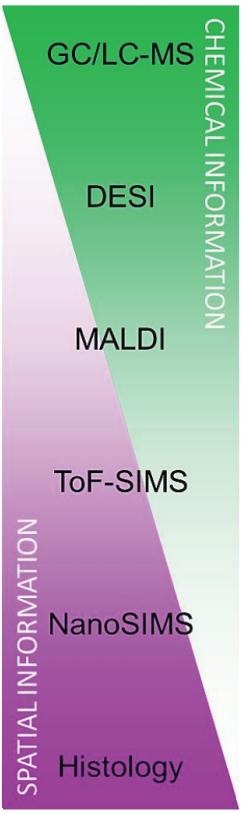

Figure 3-3 Schematic overview of spatial and chemical information provided by different techniques.

3.3.1 Histological Staining / Microscopy Techniques

Probably the first scientist to use dyes in order to reveal hidden details in samples under the microscope was Antonj van Leeuwenhoek. In the late 17th century he used saffron to stain muscle tissue.[112] Although the wide spread use of (back then natural) dyes for microscopy would take another 150 years, it can be stated that histological staining is an old technique that has led to many discoveries. Nowadays histological staining is a staple in many laboratories and hospitals (classifying cancer and determining its margins) and a wide range of dyes is available, staining for different cell and tissue components. The resolution for classical histology (using a bright field microscope with ideal setup) is limited to about 250 nm for green light (wavelength: 500 - 550 nm) due to the Abbe diffraction limit.[113] Chemical information can be gained due to the nature of the dyes, for example toluidine blue is a basic compound that preferably stains acidic tissue compounds (nucleic acid).[114] Several dyes stain lipids (oil red, sudan red, sudan black), but no dye can distinguish different lipid species effectively.[115-116]

To decouple the maximum resolution from the wavelength of the visible light, electron microscopy (such as scanning or transmission electron microscopy, SEM and TEM respectively) is an option. Instead of light it uses electrons. The resolution is better than for light microscopes due to the small de-Broglie wavelength for particles (theoretically picometer resolution).[117] To enhance the contrast in the images, either the sample has to be coated with a thin metal layer or, again dyes are used like osmium tetroxide, a lipid dye that incorporates into cell membranes and scatters electrons.[118] Although very high resolution imaging is possible with SEM/TEM, it provides mainly structural and less chemical information (similar to classical histology).

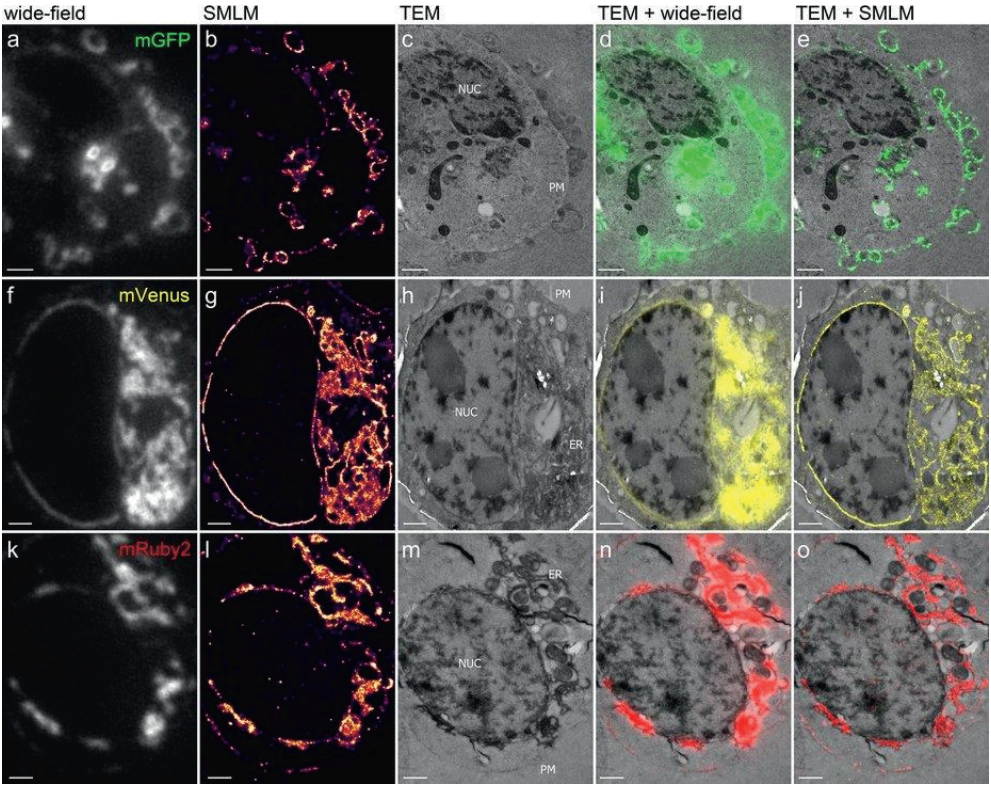

Figure 3-4 Comparison of TEM, wide-field and super resolution fluorescence microscopy images of cells. Scale bars: 1µm, License: CC-BY-0.4[119]

For better specificity, immunohistochemistry can be used. In principal, antibodies against a specific compound/protein are connected to a reporter (dye/fluorophore). The antibody will attach to its target/antigen and either the dye can be observed in the light microscope or the fluorophore is stimulated and emits light in a specific wavelength range, detect by a fluorescence-microscope. Fluorescence microscopy can be performed on live samples and several ultra-resolution methods are available (STED, PALM, dSTORM among others), improving 3-7 fold (~10-100 nm) upon the resolution of confocal microscopy.[120] The best resolution can be achieved on fixed samples. By choosing fluorophores carefully (minimal wavelength overlap), up to 4 components can be targeted and imaged in one sample. A comparison between confocal, super resolution microscopy and TEM is shown in

Figure 3-4, reproduced from Johnson, *et al.*[119]

3.3.2 NanoSIMS

NanoSIMS (CAMECA, France) is similar to ToF-SIMS in the secondary ion generation process but uses a co-axial primary/secondary ion transport system coupled with a magnetic sector mas analyser, achieving a "useful" image resolution of about 50 nm for real-life samples (in contrast to fabricated samples, specifically generated to test instrument performance). The primary ion sources for NanoSIMS (and ToF-SIMS) are not diffraction limited, which enables imaging at high spatial resolutions. ToF-SIMS lacks the sensitivity at small pixel sizes for sufficient image contrast. Therefore although 50 nm resolution is possible, for most samples it is not feasible. The NanoSIMS gets around this issue by: detecting only small secondary ions (atoms or small molecules); separating the ions in a magnetic sector mass analyser (mass resolution of several 1000, enough for small secondary ion species); instead of scanning, the NanoSIMS has a detector for each mass (up to 7); the samples are pre-treated with isotopes to be incorporated into specific parts of the sample and the images displayed are usually of isotope ratios (*e.g.* $^{15}N/^{14}N$). Positive and negative secondary ions can be detected, but require a different primary ion source (Cs^+ for negative ions, O^- for positive ions). NanoSIMS and SEM require very similar sample pre-treatment procedures, which makes them complimentary techniques providing high resolution structural as well as highly specific chemical information (depending on the success and specificity of the isotopic labelling).[121] The drawback of NanoSIMS is that usually only compounds that can be labelled can be detected. Lipid species can be imaged with NanoSIMS when lipids are first pre-labelled and then introduced into the sample.[122]

3.3.3 ToF-SIMS

The principle of ToF-SIMS is explained in detail in section 3.2 ToF–SIMS Technique. ToF-SIMS analyses are label free which means it can be used as a discovery technique but the chemical information accessible with ToF-SIMS depends on the ionisation potential of the molecules in the sample. Theoretically thousands of molecules can be studied within one experiment. Spatial resolutions in ToF-SIMS images as well as the accessible molecular information depend largely on the primary ion source (but also on instrumental setup, analysis mode, etc.). A wide range of primary ion sources are available (some of them listed in Table 3-1 and as previously mentioned), from small, mono-atomic projectiles to gas clusters containing several thousand atoms. Spatial resolution is limited by the energy spread of the primary ions, the emission current, sample topography and ultimately by the impact crater of the primary ion

and the damage cross section. So far the best spatial resolution demonstrated in ToF-SIMS images was 16 nm using Bi_3^{++} on a metal sample.[123] For the analysis of biological samples and molecular information, this resolution is not practical, as molecules are heavily fragmented and not enough secondary ions are produced per pixel for sufficient image contrast. Therefore most ToF-SIMS experiments using small clusters on biological samples are performed with a spatial resolution of 200 nm, detecting mainly atoms and small molecular fragments (< 500 Da), as shown in Figure 3-5; high spatial resolution images of the skin tissue, reproduced from Kubo *et al.*[124]

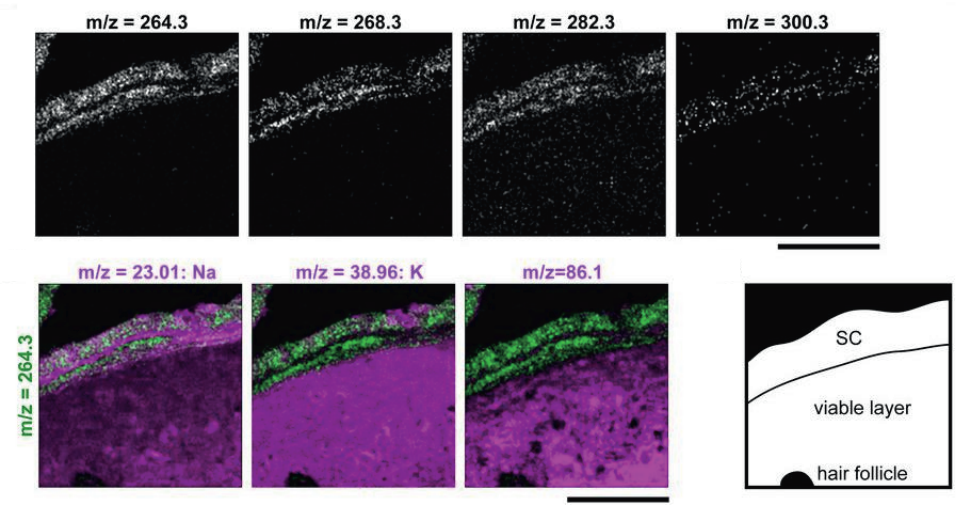

Figure 3-5 Sub-micron resolution images of skin tissue analysed by ToF-SIMS. Scale bar 50 µm. License: CC-BY-0.3[124]

While small highly energetic primary ions are easily focusable, they fragment molecules and penetrate deep into the surface, causing sub-surface damage. Part of the energy from the primary impact is transferred to the target analytes *via* atomic collisions, forming a collision cascade. Most intact molecular ions are formed at the impact crater edges and ejected from the surface due to the collision cascades. By using bigger primary ions (GCIBs) more molecular information can be gained from the samples as the energy of the primary ion is dispersed over the number of primary ions on impact on the sample surface. Bigger, shallower craters are formed and the sub-surface damage is minimised, which enables multiple analyses of the same sample surface and molecular depth profiling. The energy distribution on impact leads to a gentle removal of a

sample surface layer and less fragmentation, therefore more molecular information as demonstrated in section 6.3 Optimising Sample Preparation for Brain Sections. Detecting intact molecules is important for many reasons, *e.g.* some lipids produce the same mass fragments in ToF-SIMS but the distribution of different lipid species can give insight into metabolomics processes. The drawback of GCIBs is that the beam usually consists of a mixture of species (*e.g.* $Ar_{4000\pm500}^{+}$). This variety leads to poorer focus but imaging resolutions of a few micrometres (2-5 µm) while still detecting molecular information is possible.[4, 6]

3.3.4 MALDI-Imaging

MALDI requires a matrix and lasers to generate ion signals. Briefly, a matrix (Matrix Assisted) is deposited on a (usually tissue) sample, molecules are extracted into the matrix crystals, a Laser (see Table 3-1 for examples) is fired at the matrix, most of the lasers energy is absorbed by the matrix and the crystal "explodes" (Desorption). In the plume of ablated matrix substances the analyte molecules are ionised in the gas phase (Ionisation). With this method predominantly singly charged species are generated. The matrix has to fulfil many functions. It has to absorb the laser energy, it should form preferably small crystals, be able to co-crystallise together with the analyte and it should assist with analyte ionisation. MALDI is a soft ionisation technique, capable to lift large species off the surface but gentle enough to not fragment them during ionisation. This way, proteins above 100 kDa. in size can be imaged.[125] The spatial resolution in MALDI is limited by several factors but mainly the matrix application, the resulting crystal size and the laser. As molecules will diffuse within the crystal can their origin not be determined beyond the crystal size. Therefore the crystals have to be small enough to enable imaging at the desired resolution but also "wet" the sample enough to enable big molecules to diffuse out of the sample into the matrix droplets. In general MALDI is a very versatile technique that can be used to analyse proteins, peptides, lipids, carbohydrates and exogenous or endogenous small molecules but the choice of matrix determines what molecules can be analysed as different matrix molecules will preferentially extract/ionise different analytes. Therefore a MALDI experiment is partly a targeted approach. Although technically it is possible to image at higher resolutions (down to 1 – 2 µm),[126-127] protein MALDI imaging experiments are usually performed with spatial resolution of 50 – 200 µm (tissue wetting, crystal size, useful ion yield), lipid, peptide and small molecule imaging can be performed with 5 – 10 µm resolution.[128]

3.3.5 DESI

NanoSIMS and MALDI (and to some extend ToF-SIMS) have the disadvantage that they require sample preparation in order to introduce biological samples into vacuum, which can be very complicated and time consuming. Desorption electrospray ionisation (DESI) requires little to no sample preparation and it is an ambient technique which makes it unnecessary to freeze, dry or embed biological samples and even live samples can be studied. The technique was fist introduces in 2004, and described as follows: "*Electrosprayed (ES) aqueous droplets are directed at a surface of interest in air. The sample can be moved continuously or reoriented in space while MS analysis proceeds. The microdroplets act as projectiles and desorb ions from the surface as a result of electrostatic and pneumatic forces. The desorbed gas-phase ions are transferred to the distant mass spectrometer via an atmospheric pressure ion-transfer line.*"[88] Nowadays a variety of ambient techniques are available.[129] Similar to MALDI, a great variety of molecules can be studied and different substances can be sprayed onto the sample. The spatial resolution achievable with this technique is about 200 µm for proteins in tissue,[130] for smaller compounds ~12 µm has been demonstrated.[131]

3.3.6 Chromatography

Various chromatography methods are used to separate and identify lipids like: thin-layer chromatography, gas chromatography and most frequently used liquid chromatography (LC). LC-MS has the advantage of excellent separation of different lipid species as well as being capable of identification, structural determination (*via* MS/MS) and, to some extent, quantification of the lipids present in the sample. To perform LC-MS on a sample, it has to be homogenised and the lipids extracted using organic solvents, the lipids are separated in a LC-column, ionised using electrospray and then MS and MS/MS are performed in positive and negative ion mode.[132] Detailed information about the samples lipid profile can be acquired but due to the homogenisation, all spatial information is lost.

Chapter II: Methods

4 The J105 – *3D Chemical Imager*

All experiments in this thesis were performed on the J105– *3D Chemical Imager* which was developed in collaboration between the University of Manchester and Ionoptika Ltd (Southampton, UK) with SAI Ltd (Manchester, UK). This instrument was specifically developed as a ToF-SIMS instrument, with a re-imagined instrumental set-up, aimed at overcoming the problems many other ToF-SIMS instruments had as well as an optimisation for biological sample analysis.

At the time, the J105 was introduced (2008) conventional instruments had the drawback that one has to decide between high mass or high spatial resolution. The primary ion beam is pulsed to generate separate mass spectra from each pixel in the image. Very short pulses produce high

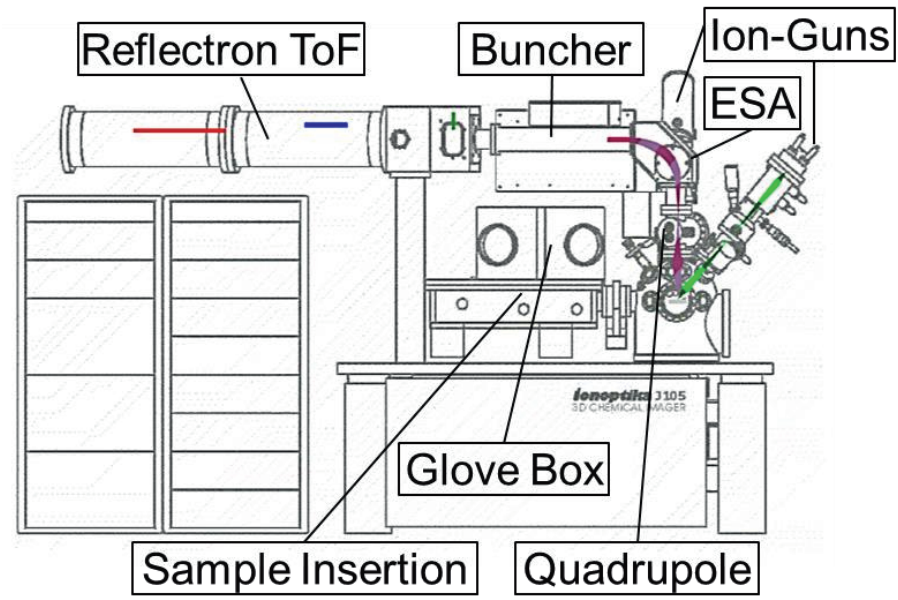

Figure 4-1 This figure shows a schematic of the J105 with the main instrumental components labelled, see text for descriptions. Continuous stream of primary ions is displayed in green, secondary ions in purple and 2 secondary ion species separated in the ToF-analyser in blue and red. Reproduced with permission from Ionoptika Ltd.

mass resolution spectra but the signal has to be generated from a bigger area, to produce enough detectable secondary ions. For high spatial resolution, long pulses from focused beams are necessary which results in a poor mass resolution. Apart from pulse length, topography can also influence the analysis quality. The J105 gets around those issues, by using a continuous primary ion beam combined with a bunched secondary ion stream which enables the generation of high spatial resolution images with high mass resolution spectra and reduced topography issues. A schematic of the instrumental set-up is shown in Figure 4-1.

In detail: A continuous primary ion beam is fired at the surface. At the time of development this beam was a 40 keV C_{60} primary ion beam operated in dc mode which produces a Wien filtered beam of C_{60} with energy up to 120 keV by selecting the C_{60}^{3+} ion. The beam can be focused to deliver an ultimate spot size of 200 nm. This beam was chosen as it was shown that C_{60} had significand advantages over small cluster liquid metal ion beams for biological analysis and organic depth profiling.[75] This continuous stream of primary ions produces a continuous stream of secondary ions, which are extracted into an radio frequency-only quadrupole filled with a suitable gas (*e.g.* N_2), where they are collissionally cooled and focussed. Then the ions are further energy filtered by an electrostatic analyser (ESA) which should provide them with an energy spread of 1 eV. An approximately 0.3 m long buncher is filled with those secondary ions which condenses the stream of ions into a narrow spot, the time focus at the entrance of the ToF-analyser. This is possible due to the buncher plates firing at the same time applying an accelerating field that varies from 6 kV at the entrance of the buncher to 0.5 kV at the exit. This causes the ions at the back of the buncher to catch up with the ions in the front but also provides them with a huge (6 keV) energy spread. This would be a problem for conventional ToF-analysers as the separation relies on all ions having very similar energy so the separation happens due to mass (to charge) differences during the flight in the field free region. Small energy differences can be adjusted by the reflectron in the end/turning point of the ToF. The J105 is equipped with a harmonic field reflectron ToF-analyser.[133] It is filled with reflectron plates and does not have a filed free region, therefore ions are separated due to their mass to charge ratios, but not their energy. The buncher-ToF setup is shown in Figure 4-2.

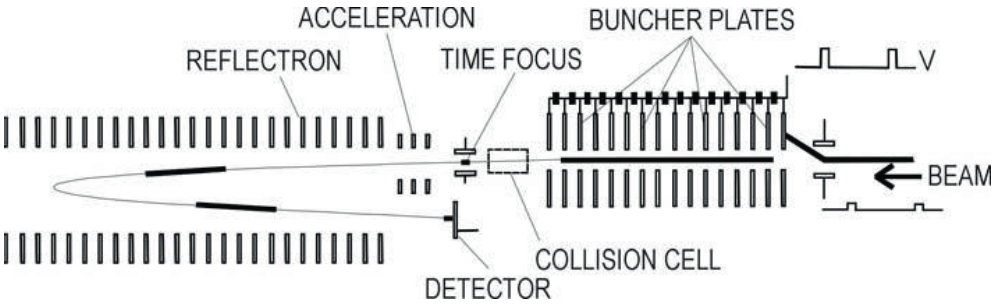

Figure 4-2 A section (~0.3 m) of the continuous secondary ion stream is bunched to a time focus and accelerated into the reflectron. The collision cell for dissociation during MS/MS experiments and several other parts are labelled.[134] Reprinted with permission from J. S. Fletcher, S. Rabbani, A. Henderson, P. Blenkinsopp, S. P. Thompson, N. P. Lockyer, J. C. Vickerman, *Anal Chem* 2008, *80*, 9058-9064. Copyright 2008American Chemical Society.

The secondary ions undergo half a period of simple harmonic motion in the analyser before impacting the detector with the same time spread as the focus achieved by the buncher, therefore the generation of secondary ions and mass resolution are completely decoupled from each other.

The J105 can produce images with sub-micron scale spatial resolution and at the same time a mass resolution of $m/\Delta m$ ~10,000 and a mass accuracy of 1-5 ppm.

Apart from those general optimisations, the J105 is especially suited for biological analysis due to a glove box on top of the sample insertion system and cryogenic sample handling. ToF-SIMS analysis happens in vacuum, therefore solid, dry samples are required but all life is based on water. One solution to this conflict is to dry the samples prior to analysis. For some samples protocols are available to make this approach feasible and still provide life-like representation but usually dehydration causes analytical problems like migration of molecules or loss of structural integrity (as discussed in section 6.1.5: Results: Optimised Sample Preparation for Single Cell Analysis and TiO2 Localisation in Cells (Paper I) and section 6.3.7: Results: TFA (Paper IV)). Fixation and embedding of samples is possible, but can lead to interferences (spectral and/or chemical) of the fixing/embedding substances with the analyte species from the sample. Flash freezing of samples and frozen analysis is the best approach to produce life-like, solid biological samples with structural integrity and without the interference of other substances but at the same time it is the most difficult to execute. If the sample is in contact with the air after freezing, ice can build up on its surface, burying the sample underneath. Also the instrument has to be kept cold at all times. The J105 can be pre-cooled, using liquid nitrogen, to about 100 K

and kept at this temperature and on top of the sample insertion port, it has a glove box. This box can be filled with an inert gas, providing a water free environment for freezing the sample, prior to inserting it into vacuum so it never comes in contact with moisture in the air.

MS/MS capability is another J105 feature which was unique to the J105 in the imaging ToF-SIMS field at the time of its introduction. This is very useful for molecular identification, to verify the peak assignment. In the J105, the MS/MS is performed in a ToF−ToF configuration. After the buncher, ions pass through a collision cells filled with gas (*e.g.* helium, nitrogen, or argon). Collision energies are in the range of 0.5−6 keV, since ions are accelerated with different energies in the buncher (as explained earlier). The collisions take place in a field-free region of the instrument which causes the parent ion and associated daughter ions to travel with the same velocity after fragmentation. A timed ion gate after a short ToF-region is used to select the parent−daughter combination of interest and admit these ions into the ToF-analyser.[134]

5 Principal Components Analysis (PCA)

Imaging ToF-SIMS produces data sets with 2D/3D images, where each pixel/voxel contains a full mass spectrum. With improving ToF-SIMS instrumentation, increasing the number and size of secondary ions detected, for intact (pseudo-)molecular ions as well as characteristic fragments, combined with enhanced mass resolution in spectra and spatial resolution in images, imaging ToF-SIMS data sets have become larger in size and increasingly more complex. Thus the use of principal component analysis (PCA), as well as other multivariate analysis techniques (such as partial least-squares discriminant analysis PLSDA, and maximum autocorrelation factors MAF) has become more popular and necessary as a means to putting the results into a comprehensible format. PCA is a variant of factor analysis, which is used to reduce the complexity of the data without loss of information and displays this variation in a number of principal components (PC), where the first principal component (PC1) captures the biggest variance in the dataset. This way the relationship between variables (*m/z* values in ToF-SIMS) and the relationship between or the separation of samples (pixels in images or sample spectra) can be identified and displayed in scores plots/images for samples and corresponding loading plots, showing the variables the scores plot/image is based on and their significance for the separation.[135] Most multivariate analysis methods are meant to be unsupervised, decision free statistical analysis tools that interpret the data without adding human bias. However decisions still have to be made as in

which method to choose, how the data is treated (normalising, scaling) prior to analysis as well as excluding outliers, areas of the image or parts of the spectra. Normalising the data as well as using suitable scaling methods is crucial to reduce artefacts from *e.g.* charging and the dynamic range in the spectra (intensity of small fragments peaks can be some orders of magnitude bigger than high mass molecular signal) and enable PCA to identify scientifically relevant features in the data. Although a wide variety of multivariate analysis methods are available and have been applied to ToF-SIMS images (and spectra), PCA continues to be the most widely used due to its availability and established history.[136-138]

MAF has been found to produce better results for images than PCA, in respect to imaging contrast and discovering key features in the data but it is also computationally more demanding.[137] Using suitable scaling methods for PCA such as root mean scaling (dividing each peak by the square root of the mean value for that peak) can produce results with similar quality to MAF and is therefore an attractive option for very large datasets. Also improved ion beam technology increases the amount of intact molecular ions detected and therefore reduces the influence of small fragments on the PCA analysis.

In this thesis, the software SIMCA, (Umetrix, Sweden) which stands for soft independent modelling of class analogy was used for PCA on ToF-SIMS spectra. This software is building models based on PCA and was used to identify the outer membrane changes in Tetrahymena due to TiO_2 nanoparticle exposure, based on spectra from single cells, shown in section 6.1.6. Additionally PCA in MatLab (The MathWorks Inc.) was used to determine *Tetrahymena* thickness for 3D reconstructions.

Imaging PCA in MatLab on square rooted data has been performed on ToF-SIMS images of brain tissue sections as shown in section 6.3.6 as well as cancer sections. Output scores images are displayed in a red-green colour scheme (showing the 2 chemically most different areas in the tissue in PC1).

Chapter III: Summary of Publications

6 Applications

ToF-SIMS analysis has many advantages as it is a technique that acquires location specific, molecular information while not requiring labels. It can therefore be used as an untargeted discovery technique. With no matrix, no labels, no extractions, theoretically the analysis process is supposed to be quite simple: acquire sample → dry (if necessary) → ToF-SIMS → other steps (*e.g.* data treatment) → results → scientific paradigm shift! However, even with this quite simplistic approach, there is a lot of scope for improvements including: sample preparation (especially for bio-samples), instrument settings, choice of ion beam; as well as things to consider when interpreting the data: necessary data treatment, matrix effects and different ionisation probabilities of secondary ion species. The ideal approach is often limited by the resources available (*e.g.* no access to fresh samples or certain instrument features not available) and can vary from sample to sample as well as it can depend on the scientific question being asked.

During this Ph.D. project different methods of sample preparation for ToF-SIMS in combination with development and application of cutting edge technology for optimisation of biological analysis, was a constant focus.

Included in this thesis:

- Single cell analysis and visualisation of cub-cellular compartments (Paper I)
- High throughput single cell outer-membrane analysis (Additional data)
- Novel GCIB technology, damage free depth profiles and matrix effects in Irganox (Paper II, Paper III)
- Sample preparation comparison for GCIB analysis on brain: freeze dried, frozen hydrated, trifluoracetic acid (TFA) or NH_3 vapour exposed (Paper II, IV, V)
- Breast cancer analysis with ToF-SIMS (Paper VI)

6.1 *Tetrahymena*: of "Small" Cells and "Big" Molecules

6.1.1 Overview

The increasing use of nanoparticles in a wide range of applications means there is a significant chance that these chemicals may enter the aquatic environment. TiO_2 is among the most produced as well as the most extensively studied nanoparticle species at the moment but there is no general consensus within the scientific community about its toxicity or its interactions with different organisms. In an attempt to add to this pool of knowledge the effects of TiO_2 nanoparticles on the fresh water dwelling single cell organism *Tetrahymena pyriformis* were studied. This organism is a popular model for toxicology studies where assays normally focus on the physical behaviour of the organism (motility, proliferation *etc.*) or where chemical analysis has been performed, large numbers of cells have been combined for analysis. Combining cell signal can show the overall treatment response from the whole culture/population but there is a risk of missing underlying effects as well as including outliers or contaminations into the analysis as illustrated in the schematic in Figure 6-1.

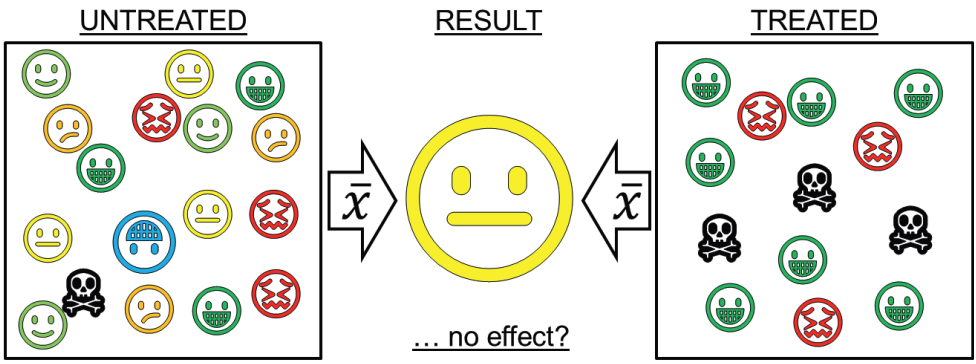

Figure 6-1 Schematic of cells in different conditions, from very active and healthy 😀 to dead ☠, within one treated (right) and untreated (left) cell culture. Distributions for different conditions vary but summed up results are the same.

SIMS offers the opportunity for studying this unicellular organism directly in order to localise the nanoparticles within the cells and show chemical effects on the outer membrane. The capability of SIMS for localising and identifying metallic/inorganic and organic compounds at the same time has been demonstrated successfully in 2D (*e.g.* titanium implants in bone)[139] but

3D analysis of mixed organic/metallic samples poses additional challenges due to different sputter rates.

Summary of results from this study:

- To keep sub-cellular structures intact without chemical fixation, frozen hydrated analysis of cells is necessary.
- Nanoparticles are accumulating in *Tetrahymena* food vacuoles that are approximately 5 µm in diameter and distributed throughout the cell.
- Sputter rates through TiO_2 filled vacuoles are reduced compared to nutrient filled vacuoles/the rest of the cell.
- TiO_2 influences fatty acid saturation observed in DAGs on the outer cell membrane.
- PCA analysis reveals 2 distinct treatment responses in the cell culture.

6.1.2 *Tetrahymena*

The ciliate *Tetrahymena* are considered one the most highly developed protozoa organism because of specialised organelles that perform different cellular functions and a metabolism comparable to higher organisms. They have been used as model organisms in scientific studies for several decades. They are well characterised, fresh water dwelling, unicellular eukaryotes that are very adaptive to their environment and inhabit most fresh water habitats on the planet. The capability of adjusting to many non-favourable conditions (pH and temperature changes, lack of nutrients, contaminants) and the easy handling (grows to high cell numbers, no need for aseptic conditions) has made *Tetrahymena* a popular study target in many fields.[140] Especially the species *Tetrahymena pyriformis* has been used for studies in toxicology.[141]

Apart from its adaptiveness and simple handling it is its size of approximately 40 µm that makes *Tetrahymena* an ideal target for ToF-SIMS studies. Previously published studies have focused on changes in lipid composition during cellular events such as mating[142] and cell division.[143]

6.1.3 TiO_2 Nanoparticles

Titanium dioxide (TiO_2-NP) nanoparticles have various applications, such as self-cleaning surface coatings, light-emitting diodes, disinfectant sprays and topical sunscreens.[144-146] Estimates for the commercial production of TiO_2 are as high as 2.5 million tons by 2025[147] so it is to expect that release and thereby the exposure of TiO_2 to the environment will enhance

significantly, as indicated by the present TiO_2-NP discharge from façade paints into surface waters.[148] Environmental exposure of TiO_2-NP caused by consumer products are predicted to be 24.5 µg/l for water and 1030 µg/kg for soil.[149]

Although TiO_2 is the most studied metal oxide nanomaterial there is no general consensus if TiO_2 nanoparticles are toxic.[150-151] Natural NPs, including nano-sized particles of metal oxides, exist in all ecosystems and play important roles in biogeochemical processes.[152] For the toxic effects of TiO_2-NPs on organisms that have been observed, secondary particle size, the surface chemistry and the duration of exposure seem to be the most important parameters.[153-155] Organisms have evolved to adapt to the presence of natural NPs in the environment, however it has been recognised that synthetic NPs are potentially harmful for ecosystems and need to be studied carefully.[156] ToF-SIMS can be used for the detection and characterisation of nanoparticles and their effect on organisms but this approach is not without challenges.[157-158]

6.1.4 Summary of Methods

For this study TiO_2 anatase nanoparticles with a 22 nm diameter and a final concentration in the media of 16 µg/ml were used. NPs were added to freshly propagated *Tetrahymena* in media, grown for 24 h and then washed in ammonium formate to remove extracellular media salts while maintaining the osmotic pressure.

Sample preparation: Washed cells were spotted on a silicon wafer and either dried in air or prepared frozen hydrated with liquid nitrogen. For frozen hydrated analysis, the sample insertion and analysis stage of the J105 were cooled down and maintained at 120 K during the analysis. All experiments were performed using a 40 keV C_{60}^+ primary ion beam (Ionoptika Ltd, U.K.).

Outer membrane changes: Freeze dried cells were analysed with 40 keV C_{60}^+, surface spectra for all individual cells were extracted manually by summing up the signal from all pixels corresponding to one cell, spectra were normalised to their total ion signal and principal component analysis (PCA) was performed on the whole dataset (all cells, treated and untreated) in SIMCA (Umetrix, Sweden).

6.1.5 Results: Optimised Sample Preparation for Single Cell Analysis and TiO_2 Localisation in Cells (Paper I)

6.1.5.1 Sample treatment

Displayed in Figure 6-2 are the distributions of different molecules within *Tetrahymena* grown without TiO_2-NP exposure and analysed with ToF-SIMS under different conditions (b) dried, (c) semi dry and (d) frozen hydrated. Only in panel (d) a clear distribution and sub-cellular compartmentalisation can be seen wile in (b) all sub cellular structures are lost. Panel (c) shows an intermediate state where a cell is exploding while drying out which explains the loss of structure in (b). Since the goal of this study was to study TiO_2 localisation as well as chemical changes due to exposure chemical fixation was avoided as it might changes cell chemistry. The initial result on unexposed cells showed, that frozen hydrated analysis was necessary.

The unexposed cells contained multiple sub cellular structures, roughly 5 µm in size and with chemical signatures different from the rest of the cell but similar to the cell media. Size, number and content made it apparent that those structures were the food vacuoles inside the cell as shown in (a) (multiple round structures inside the cell).

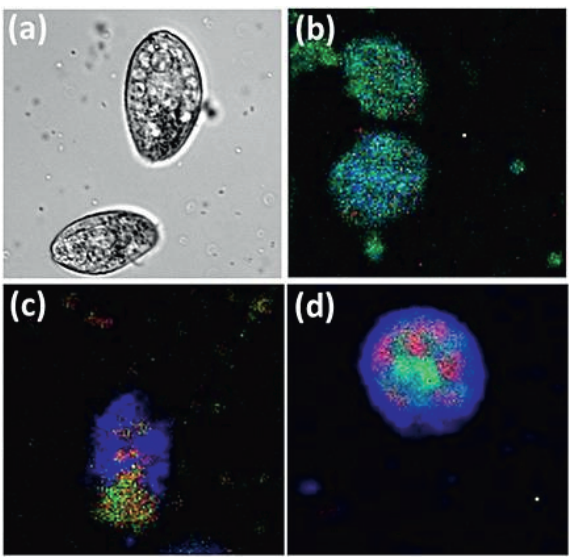

Figure 6-2 (a) Optical image of *Tetrahymena* and *Tetrahymena* imaged by ToF-SIMS following three different sample preparation methods. (b) Dried and analysed at room temperature, negative ion image m/z 101.05 (red), *m/z* 198.95 (blue) and *m/z* 158.95 (green) none of the peaks show clear localisation within the cell. (c) Partially dried at room temperature then analysed frozen, positive ion image shows rupture of the cell *m/z* 212.80 (red) *m/z* 156.00 (green) and *m/z* 184.10 (blue). (d) *Tetrahymena* analysed in a frozen-hydrated state, negative ion mode image *m/z* 101.05 (red), *m/z* 198.95 (blue) and *m/z* 158.95 (green). The same species as in panel (b) are displayed but now with clear localisation. Each image is 128×128 µm^2, 128×128 pixels, acquired using 40 kV C_{60}^+. The images show each cell after removal of the outer membrane by etching with C_{60}^+. Reproduced with permission from T. B. Angerer, J. S. Fletcher, *Surf. Interface Anal.* 2014, 46, 198-203. Copyright 2014 Wiley.

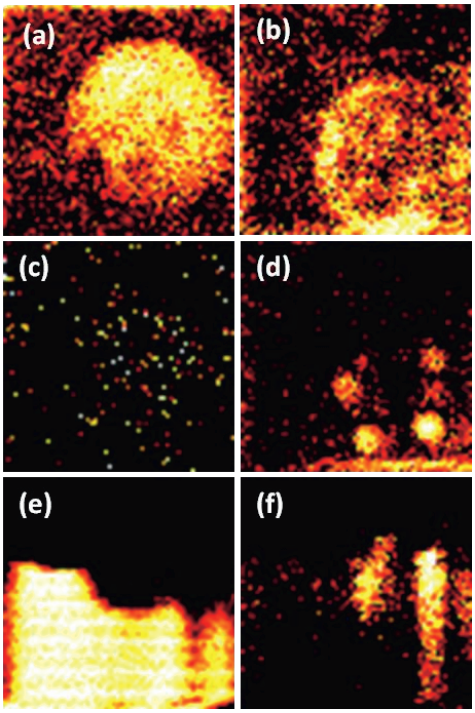

Figure 6-3 x–y plane images of *m/z* 184.10, phosphatidylcholine, signal distribution on the surface of a *Tetrahymena* (a) and inside a *Tetrahymena* following C_{60}^+ etching (b) *m/z* 63.95, $[TiO]^+$ intensity distribution on the surface of a *Tetrahymena* (c) and inside a *Tetrahymena* following C_{60}^+ etching, 4×10^{15} ions/cm^2 (d) x–z slices through a stack of images acquired of *Tetrahymena* exposed to nanoparticles showing the silicon substrate, *m/z* 167.9, Si_6^+ (e) and the m/z 63.95 , $[TiO]^+$ (f) A substantial difference in sputter rate is apparent between the cell body and the nanoparticle-rich regions. Images acquired using 40 keV C_{60}^+ over a field of view of 70×70 µm^2 with 64×64 pixels. Reproduced with permission from T. B. Angerer, J. S. Fletcher, *Surf. Interface Anal.* 2014, 46, 198-203. Copyright 2014 Wiley.

6.1.5.2 TiO_2 exposure

Figure 6-3 shows organic and titanium oxide signals from the cell surface (a, c) and after C_{60}^+ etching (b, d). When analysing TiO_2 exposed cells, titanium oxide related signals were found to be co-localised with vacuole contents in multiple round compartments (d) inside the cell, but not on the outer cell membrane (c) or outside the cell. This indicates that the titanium signals come from inside food vacuoles, as all excess TiO_2 has been washed away. This suggests that TiO_2 is forming aggregates with the media (nutrients from yeast extract) which are then consumed by the *Tetrahymena* cells but the nanoparticles do not seem to attach to the cell surface.

Apart from the localisation it was also observed that titanium containing vacuoles have sputter rates different from food/salt containing ones and the rest of the cell. This makes it appear as if the vacuoles are protruding into the silicon substrate (e, f) whereas under the microscope vacuoles of exposed cells show no deformations compared to the control cells.

6.1.5.3 Additional Data Not Included In Paper I

Analysis of multiple cells showed that all exposed cells contained titanium within their food vacuoles as well as that the degree of sputter rate related vacuole deformation depends on the amount of titanium inside the vacuole. Figure 6-4 shows that vacuoles containing only small

amounts of titanium (as indicated by the yellow, lower intensity TiO^+ signal in (c)) still appear as spherically shaped (yellow vacuoles) while higher intensity vacuoles (orange) are elongated and very high intensity vacuoles (red) were not entirely sputtered away within the timeframe of the experiment and remained long after all other cellular components were removed. The 3D models show the localisation of titanium oxide and the depth profiles in (c) the corresponding depth profiles, showing the increasing intensity in titanium oxide signals for those vacuoles that are the most deformed.

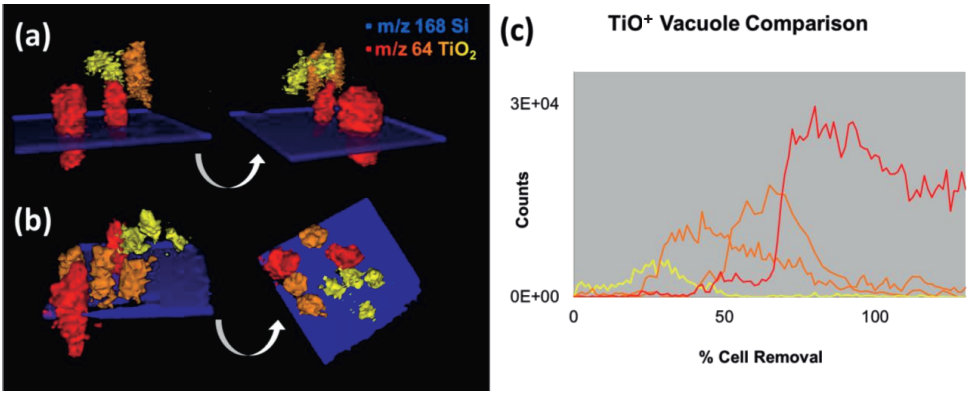

Figure 6-4 Z-corrected 3D reconstruction of 2 nanoparticle treated *Tetrahymena* cells, with only the vacuoles and substrate displayed from 2 angles each. Cell (a) is the same cell as shown in **Figure 6-3**. Displayed in blue is the first silicon layer (*m/z* 167.86, Si_6^+) the cell resides on. Titanium inside the cell vacuoles (*m/z* 63.94, TiO^+) is displayed in yellow (low intensity signal), orange (medium) and red (high intensity). The same colour scheme is adapted in the depth profiles in (c) where the intensity of titanium signal is plotted as a function of % cell removal.

6.1.6 Results: Outer Membrane Changes due to TiO_2 Exposure

For singe celled organisms the cell membrane is the barrier between them and their environment. As mentioned, *Tetrahymena* is known to adapt quickly to environmental changes *e.g. via* membrane lipid changes. Although not extensively investigated, after 24 h TiO_2 exposure no behavioural (fewer numbers, less agility) or physiological changes (cell shapes or sizes) were observed in treated *versus* control cells. The question was, even if TiO_2 exposure does not seem to change the cells visibly, does internalising TiO_2 have chemical effects, leaving the outer cell membrane barrier altered and possibly more vulnerable to other influences?

Although drying the cells damaged internal structures, the outer cell membrane stayed largely intact. Therefor to investigate the effect that internalised titanium oxide had on the cell

membrane, the measurements were conducted on dried cells. This enabled the analysis of larger cell numbers over a longer time, which would not be feasible in frozen hydrated studies.

Figure 6-5 (a) shows the resulting PCA scores plot PC1 versus PC4 from this analysis, as well as the loadings for PC1 and PC4 in the background. Each measurement/sample on the scores plot represents one cell. Panel (b) and (c) are 2 example images from where the spectra were extracted. PC4 separates treated (THTi) and untreated (TH) cells and the loadings show that mainly diacylglyceride (DAG) signals are responsible for the separation. The table to right shows

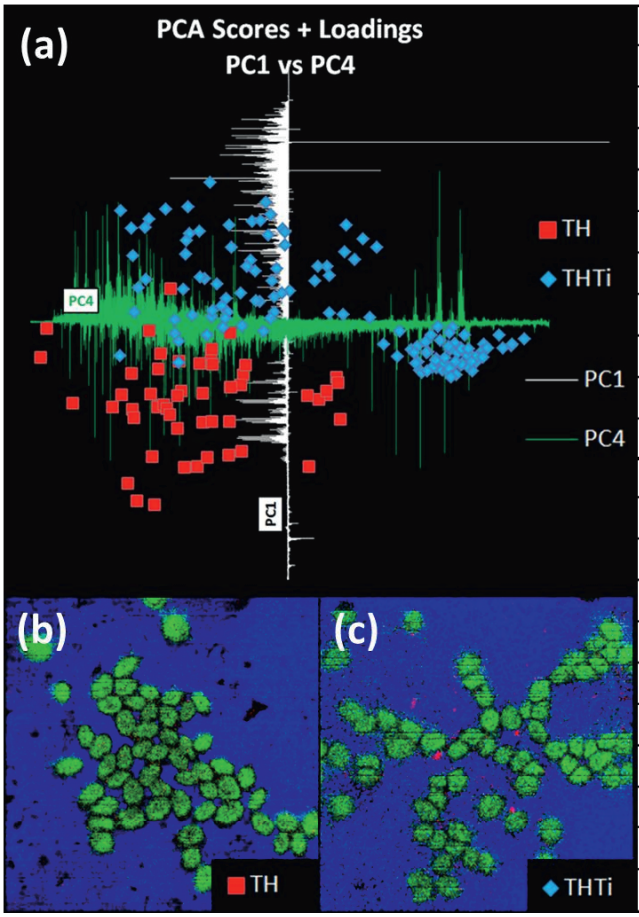

PC4 +	
m/z	Species
559.47	DAG(33:3)
561.47	DAG(33:2)
569.46	DAG(32:0)
571.55	DAG(34:4)
573.57	DAG(34:3)
575.54	DAG(34:2)
597.51	DAG (36:5)
599.52	DAG (36:4)
601.53	DAG (36:3)
PC4 -	
m/z	Species
549.50	DAG(34:1)
551.49	DAG(34:0)
563.54	DAG(33:1)
565.56	DAG(33:0)
577.57	DAG(34:1)
579.54	DAG(34:0)
593.57	DAG(35:0)
605.55	DAG (36:1)
607.57	DAG (36:0)

Figure 6-5 PCA on single cell spectra comparing spectra from treated (blue, THTi) and untreated (red, TH) cells. (a) Scores plot PC1 *vs.* PC4 with loadings for PC1 (white) and PC4 (green) in the background, *m/z* 50-950; positive ion ToF-SIMS overlay image of untreated (b) and TiO_2 exposed *Tetrahymena* showing TiO^+ (*m/z* 63.94, red), PC-head-group (*m/z* 184.07, green) and silicon substrate (*m/z* 167.86, blue).The table to the right shows signals corresponding to positive and negative loadings in PC4.

the peak masses and putative assignments of the main species responsible for separating the cells. Untreated cells are high in saturated and monounsaturated species while treated cells mainly contain polyunsaturated species. Interestingly the TiO_2 exposure seemed to create 2 subgroups; the majority showed the changes described above and the 2nd group did not produce many DAG signals but showed increased phospholipid content.

This highlights the importance of single cell analysis, since this trend could not have been observed by analysing lipid extracts from multiple cells. The biological reasons for the saturation change as well as the 2 distinct response patterns are currently unknown.

6.1.7 Conclusion: *Tetrahymena*

ToF-SIMS analysis with C_{60}^+ as primary ion beam is capable of localising subcellular structures in 3D in frozen hydrated *Tetrahymena* as well as generating molecular profiles for single cells, exposing differentiated treatment responses.

6.2 Novel GCIB Technology tested on Irganox: BIGGER IS ALWAYS BETTER.

6.2.1 Overview

In 2014 the world's first 40 keV high energy gas cluster ion beam (GCIB) was fitted onto the J105. Most commercially available GCIBs operate with energies up to 20 keV. The main advantage of using GCIBs for ToF-SIMS is less fragmentation due to a "softer impact" as the energy is distributed between the atoms in the cluster upon impact on the surface. This makes ToF-SIMS more applicable for organic samples, containing large (500-2000 Da) and fragile molecules. The concern was that when using GCIBs at higher energies the benefits of the softer impact would be negated by the added energy and lead to increased fragmentation and sub surface damage accumulation.

To test these concerns experiments using different cluster sizes and energies were performed on Irganox1010, an extensively studied standard material, which consists of one large molecule that can be detected as intact molecule alongside characteristic fragments. Hence the results would be comparable to previously performed beam characterisation studies. Also, as participation in an inter-laboratory study, experiments on mixed materials were performed to study the severity of matrix effects during depth profiles using different primary ion sources.

Summary of results from those studies:

- 40 keV GCIB analysis does not lead to increased fragmentation of Irganox 1010 or to accumulated damage in depth profiles.
- Sputter rates and primary beam energy are directly proportional while cluster size has less influence.
- Ionisation efficiency decreases rapidly when the beam energy is below 5 eV per atom.
- Signal intensity increases with increasing beam energy due to more material being removed, not due to improved ionisation efficiency (above 5 eV/atom).
- Matrix effects on Irganox/F-moc samples are more severe when using argon gas clusters compared to bismuth, during depth profiling.

6.2.2 Irganox 1010

Irganox 1010 is a large tetrahedral molecule that is often used as an antioxidant, with a central carbon atom bound to 4 arms with a mass of 291 Da. each. The ToF-SIMS spectrum of Irganox shows many characteristic peaks (*e.g.* corresponding to the loss of each arm) up to its *pseudo*-molecular ion at *m/z* 1175 $[M-H]^-$. Irganox 1010 has become a popular test sample in SIMS studies to investigate the characteristics of different ion beams in respect to sputter rate, depth resolution and ion yield.[77, 159-161] Also it is used for molecular depth profiling as it is stable under vapour deposition conditions, allowing uniform films to be formed. For example in a VAMAS study, organised by the National Physical Laboratory (NPL, Teddington U.K.), an Irganox 1010/ Irganox 3114 test sample was used for molecular depth profiling to characterise the performance of several ion beams (predominantly C_{60}) and analysis conditions.[162] The use of low energy Ar_n^+ cluster ion beams can further improve depth resolution and signal stability, as was shown in follow up study.[163]

6.2.3 GCIBs for Analysis and Depth Profiling

The benefits of Ar_n^+ clusters for depth profiling of organic materials, have led to almost all new ToF-SIMS instruments being equipped with a GCIB as well as considerable interest from the XPS field for GCIBs as sputter beams.[164] Several ToF-SIMS studies have been performed to establish sputter rates through different types of materials, e.g. for gold[165] and the previously mentioned Irganox 1010/ Irganox 3114 sample.[163]

There are considerable benefits for the use of GCIBs for biological sample analysis, *e.g.* increased signal persistence during depth profiles of tissue samples when using Ar clusters for

either etching and analysis[166] or just for etching with interleaved Bi_3^+ analysis. This can lead to a potential 100× signal increase compared to standard analysis.[167] Although there are clear advantages to the use of GCIBs the optimum operational parameters of those ion beams have not been verified. Most existing data is from GCIBs as etching but not analysis beams. In studies where they have been used for analysis, several general observations have been reported, such as less fragmentation and increased higher mass species.[100] The downside is that overall secondary ion yields can be low as ionisation is often less efficient and one has to be aware that due to the reduced energy per atom characteristic fragments and overall signal can drastically change as shown for polystyrene.[81, 168]

6.2.4 Summary of Methods

Beam performance study: A 48.54 nm thick Irganox 1010 sample was analysed with using different cluster sizes of Corgon (8% CO_2, 92% argon, for simplicity the clusters will be referred to as Ar_n^+) and beam energies until the Irganox layer was completely removed. Energies: 10 keV, 20 keV, 30 keV and 40 keV; Cluster sizes: Ar_{1000}^+, Ar_{2000}^+ and Ar_{4000}^+

Matrix effects study: 2 samples were analysed using Ar_{4000}^+ at 40 keV. MMF sample: pure and mixed layers of Irganox 1010 and FmocPFLPA; MMK sample: pure and mixed layers of Irganox 1010 and Irganox 1098.

For both studies samples were supplied by NPL, UK.

6.2.5 Results: Beam Performance (Paper II)

Figure 6-6 (a) shows that sputter rate and beam energy (or acceleration potential) are directly proportional to each other; with half the beam energy it takes twice as many primary ions to remove the same amount of material. This trend is seemingly independent of the cluster size, therefore not correlated to the energy per atom except for a slight deviation from this linear trend when the energy drops below 5 eV/atom. The observations are in agreement with other GCIB studies.[169-170]

Panel (b) shows the depth profiles for 40 keV energy and 3 cluster sizes. As indicated in panel (a) the 3 cluster sizes have little influence on the total ion dose needed to remove the Irganox layer but, what is important, is that it is possible to produce stable depth profiles based on the molecular ion with all cluster sizes (no accumulated damage observed). A slight influence of cluster size can be seen since the analysis is “fastest” with Ar_{1000}^+ 40 keV (= 40 eV/atom) and

slowest with Ar_{4000}^+ 40 keV but while the 40 keV analyses all require approximately 1 × 10^{13} ions/cm^2 , the 20 keV analyses require 2 × 10^{13} ions/cm^2. To summarise plots (c-f): there is no significant increase in fragmentation when using 40 keV but a 2 fold gain in signal (e, f) compared to 20 keV. Below 5 eV/atom the signal drops off non-linearly/more than just due to the reduced sputter rate with lower beam energies (*e.g.*: (e) Ar_{4000}^+ 20 keV produces signals with about 20% intensity compare to 40 keV but it should be half, since at 20 keV half as much material is removed compared to 40 keV).

At 2.5 eV/atom hardly any signals are detected ((e) Ar_{4000}^+ 10 keV) and the sputter rate decreases disproportionally as well but material is still removed. This shows that the threshold for linear sputter efficiency (2.5 eV/atom) is lower than for ionisation efficiency (5 eV/atom). Therefor the first advantage when using 40 keV GCIBs is that one can use bigger clusters as primary ions without suffering from ionisation efficiency loss. The second advantage is improved beam focus (< 3 µm for Ar_{4000}^+).

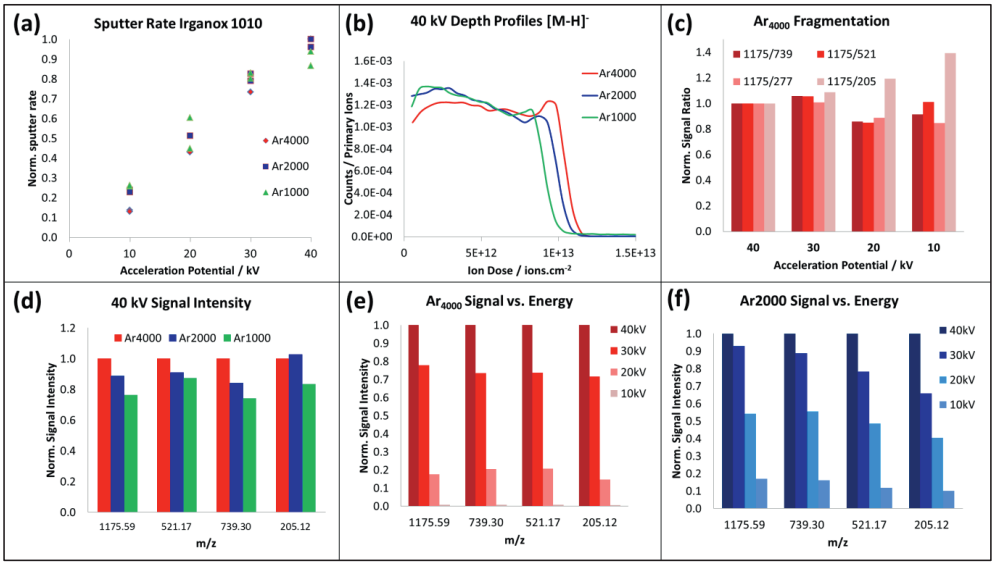

Figure 6-6 Results of the analysis of Irganox 1010 using Ar_n^+ (n = 1000, 2000 and 4000) at 10, 20, 30 and 40 kV acceleration potential. Relative sputter rates normalised to 40 keV Ar_{4000}^+ (a), $[M-H]^-$ ion depth profile plots (b), normalised fragment ratios (c), relative signal levels for different cluster sizes using 40 kV acceleration potential normalised to Ar_{4000}^+ (d), relative secondary ion signal variation under Ar_{4000}^+ bombardment as a function of acceleration potential (e) and relative secondary ion signal variation under Ar_{2000}^+ bombardment as a function of acceleration potential (f). Reprinted with permission from T. B. Angerer, P. Blenkinsopp, J. S. Fletcher, *Int. J. Mass Spectrom.* 2015, 377, 591-598. Copyright 2015 Elsevier.

6.2.6 Results: Matrix Effects (Paper III)

As participation in a VAMAS inter-laboratory study, coordinated by NPL, 2 samples were analysed, composed of pure and mixed layers of different polymers. To find out the composition other participants used different primary ion species and energies. The results from those depth

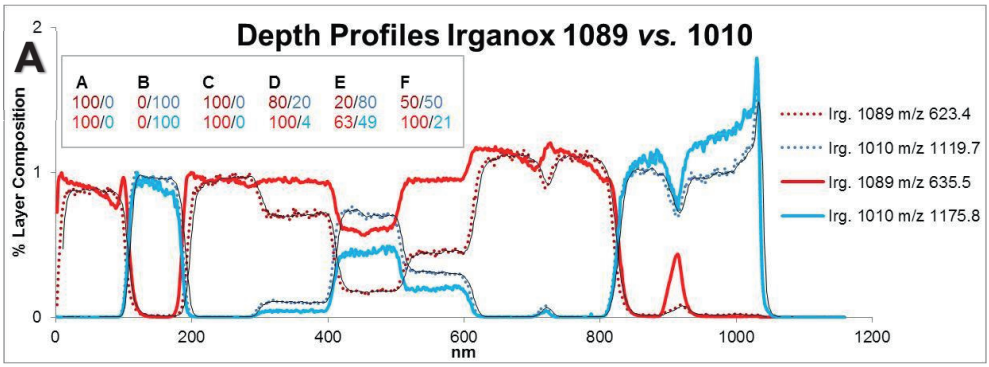

Figure 6-8 A Depth profile of 1056 nm thick NPL sample MMK (SRTABZ) composed of alternating, pure and mixes layers of Irganox 1010 and Irganox 1089; plotted are Irg. 1010 $[M-H]^-$, *m/z* 1175.8, Irg. 1010 fragment, *m/z* 1119.7, Irg. 1089 $[M-H]^-$, *m/z* 635.5 and Irg. 1089 fragment, *m/z* 623.4. Each depth profile is normalised to an average local maximum between 5-30 nm. The table in the graph shows the actual composition above each layer (A-F) as % Irg. 1089/% Irg. 1010 in the top row and the measured composition based on the molecular ion signal in the bottom row.

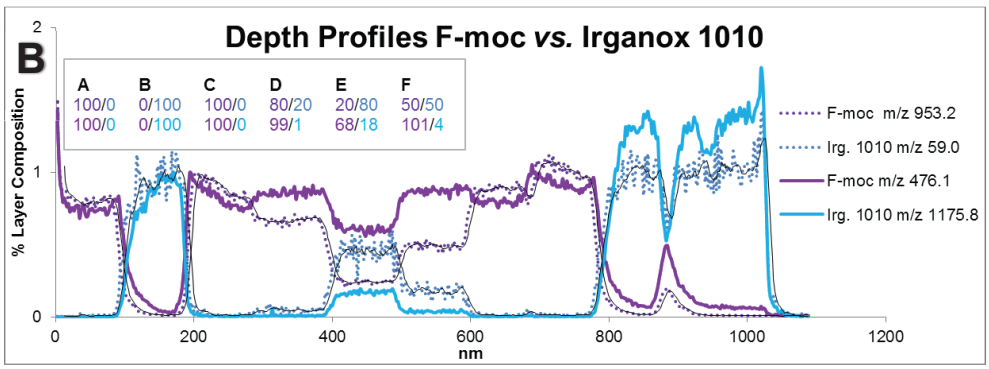

Figure 6-8 B Depth profile of 1056 nm thick NPL sample MMF (SRT5AI) composed of alternating, pure and mixes layers of Irganox 1010 and F-moc; plotted are Irg. 1010 $[M-H]^-$, *m/z* 1175.8, Irg. 1010 fragment , *m/z* 59.0, F-moc $[M-H]^-$, *m/z* 476.1 and F-moc species $[2M-H]^-$, *m/z* 953.2. Each depth profile is normalised to an average local maximum between 5-30 nm. The table in the graph shows the actual composition above each layer (A-F) as % F-moc/% Irg. 1010 in the top row and the measured composition based on the molecular ion signal in the bottom row.

profiles are displayed in Figure 6-8. The aim was to determine the composition of layer D and E, while A, B, C and F were known (as well as an ideal depth profile without values was provided) and to report the ratios corresponding to different fragments. After reporting back the results, the real composition was revealed.

Different fragments would result in different ratios, some following the provided ideal depth profile, some showing more than 100% intensity in a mixed layer and deviating significantly from the ideal profile. It was observed that mixtures of Irganox 1010 with Irganox 1089 or F-moc would result in matrix effects, reducing the signal intensity of Irganox 1010 while enhancing the signals of Irganox 1089 and F-moc respectively. Figure 6-8 A/B each show the fragment of each species that follows the ideal profile most closely, compared to the molecular ion signal, where matrix effects are observed. This effect was observed by all participants in the study but matrix effects were more severe in GCIB profiles, compared to *e.g.* Bi_3^+.

6.2.7 Conclusion: Irganox

40 keV GCIB analysis on Irganox does neither lead to increased fragmentation relative to the signal intensity, nor accumulated damage in depth profiling due to the high acceleration potential but GCIB analysis in general can intensify matrix effects. Despite the high energy the 40 keV GCIB analysis showed the highest depth resolution

6.3 Optimising Sample Preparation for Brain Sections

6.3.1 Overview

In previous studies tissue analysis with GCIBs lead to less fragmentation and "cleaner" spectra (*e.g.* 20 keV Ar_{2000}^+ compared with C_{60}^+).[92] The concerns about the destructive nature of a 40 keV GCIB proved unfounded on standard Irganox but do those observations apply to biological samples as well? To answer this question, similar experiments were performed on rat brain tissue sections and the results were similar: an increase in lipid signal with higher energies. This applied to all lipids except cholesterol which has been shown to migrate to the surface where it crystallizes (unless the tissue is analysed frozen),[171-172] therefore its signal is disproportionally enhanced in ToF-SIMS compared to other methods and what is reported in the literature.[173] The cholesterol migration leads to low signal intensities for other lipid species in the white matter. To produce a more life-like representation of lipid signals in various important

brain regions (striatum, hippocampus and cerebellum), different sample preparation techniques were tested for their ability to enhance the signal even further and remove artefacts, such as cholesterol surface enrichment: frozen hydrated analysis was compared with freeze drying followed by trifluoroacetic acid (TFA) and ammonia (NH_3) exposure, prior to analysis.

Summary of results from those studies:

- Increased lipid signal from brain samples with 40 keV Ar_{4000}^+ > 40 keV Ar_{2000}^+ > 40 keV C_{60}^+
- Cold analysis of fresh frozen hydrated brain sections gives the highest intensity signals and most accurate lipid profile representation.
- TFA treatment removes cholesterol crystals from the sample surface, enhances signals in positive ion mode and gives rise to previously unobserved species in ToF-SIMS.
- NH_3 treatment partially removes cholesterol.

6.3.2 Trifluoracetic Acid (TFA)

Trifluoracetic acid (TFA) was selected for tissue exposure as it is a common additive to MALDI matrices to aid ionisation as a proton donor. There have been previous reports of ion enhancement in SIMS using diluted solutions of TFA. Incubation with TFA or application of diluted TFA to the surface of samples of polyurethanes[174] and insulin[175] showed significant signal enhancement. The use of TFA vapour for SIMS was demonstrated by the Winograd group where the TFA was used to break the bond between polystyrene beads and peptide coatings.[176] TFA applied by inkjet printing[177] or spraying[178-179] has been used to enhance peptide and protein signals in SIMS studies.

6.3.3 NH_3

While acidic TFA vapour acts as a proton donor, increasing protonated $[M+H]^+$ species in positive ion mode, basic ammonia vapour from solution should act as proton acceptor, increase deprotonated $[M-H]^-$ species in the ToF-SIMS spectra. Ammonia vapour has been previously used by Vaidyanathan and co-workers to successfully increase the intensity of deprotonated secondary ion species from small plant metabolite cocktail drops.[180] In MALDI experiments ammonia salts have shown to provide samples with negative charges.[181]

6.3.4 Summary of Methods

Rodent brain was sectioned in a cryomicrotome (Leica CM1520) in the MS lab, mounted onto ITO-coated glass, freeze dried and analysed with different primary ion beams 40 keV Ar_{4000}^+, 40 keV Ar_{2000}^+, 40 keV C_{60}^+ (analysed area: striatum); analysed with 40 keV Ar_{4000}^+, frozen hydrated without being thawed prior to analysis (hippocampus), dried and exposed to TFA (cerebellum) or freeze dried and exposed to NH_3 (hippocampus) for 15, 30 and 60 minutes each. Freeze dried brain sections were used as comparison for all white and grey matter regions.

6.3.5 Results: Beam Comparison on Brain Tissue (Paper II)

Figure 6-9 shows a clear increase in molecular signal when the GCIB was used compared to C_{60}^+. The highest intensity can be achieved when using 40 keV Ar_{4000}^+, due to a combination of an increased sputter rate and a gentler impact. Therefore we can conclude that tissue samples follow the same trends as Irganox when analysed with high energy GCIBs. Notably the intensity of ganglioside signals (GM1, *m/z* 1544.87) increased to a level that it becomes possible to image these species. Cholesterol does not follow this trend due to cholesterol migration to the surface and crystallisation. $C_{60}^+$is better suited for breaking up those crystal structures than giant gas clusters and therefore shows higher cholesterol signals in the spectrum as well as the most intense (brightest) cholesterol signal in the image. Cholesterol migration is problematic as it leads to an over representation of cholesterol in the tissue, especially in the white matter, while other signals are masked. To find a way around the cholesterol problem, several approaches were successful: Frozen hydrated analysis and TFA/NH_3 vapour exposure.

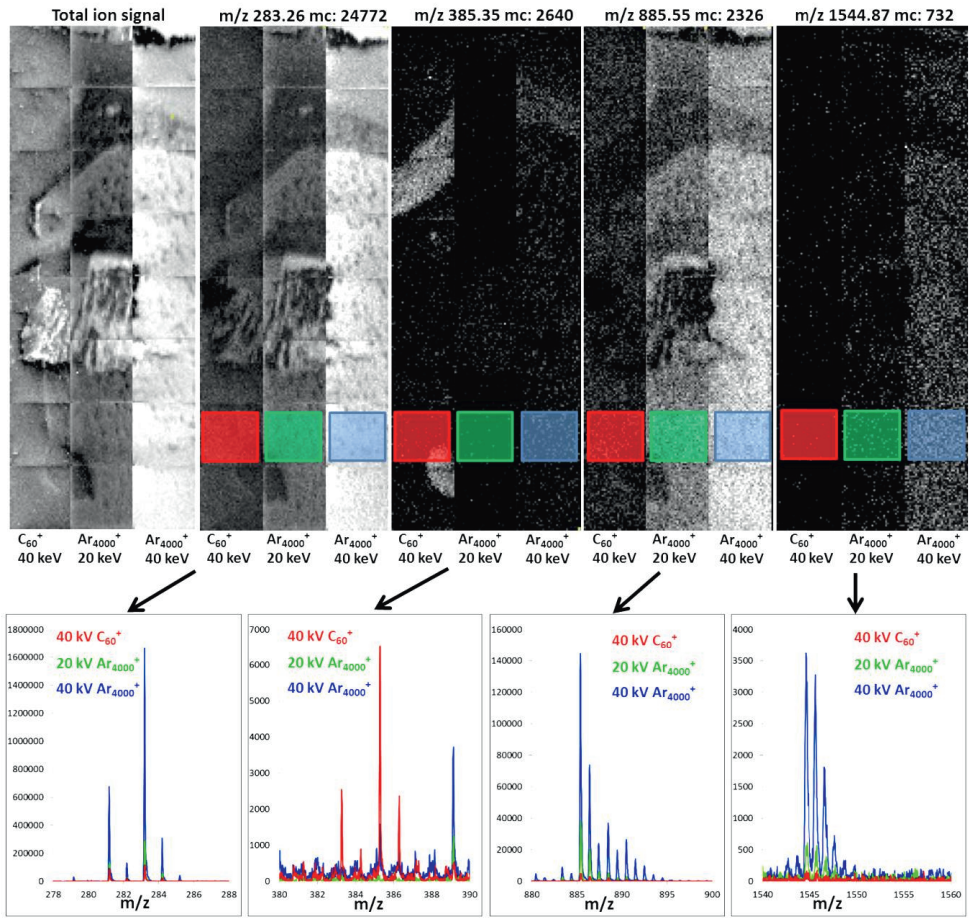

Figure 6-9 Negative ion mode ToF-SIMS imaging of mouse brain using 40 keV C_{60}^+, 40 keV Ar_{4000}^+ and 20 keV Ar_{4000}^+. Each beam was used to analyse a vertical strip of the tissue section in stepped stage mode. Each strip comprises 8 individual 800 × 800 μm^2 images with 32 × 32 pixels. All images were acquired with the same primary beam dose density of 1.44 × 10^{11} ions/cm^2.The total ion image is displayed in the left panel and to the right individual ion images are shown for *m/z* 283.26, *m/z* 385.35, *m/z* 885.55 and *m/z* 1544.87 to highlight the variation of signal intensity as a function of mass. Excerpts of mass spectra showing the imaged peak are placed at the bottom of the figure where the signal was integrated over the colour coded regions in the images. Reprinted with permission from T. B. Angerer, P. Blenkinsopp, J. S. Fletcher, *Int. J. Mass Spectrom.* 2015, 377, 591-598. Copyright 2015 Elsevier.

6.3.6 Results: Frozen Hydrated Tissue Analysis (Paper V)

Frozen hydrated tissue analysis prevents the problems caused by cholesterol migration and increases overall lipid signal. Cholesterol, which is found in all cell membranes, is detected almost evenly distributed in the tissue, while the white matter is dominated by sulfatide signals in negative ion mode and ceramide signals in positive ion mode. The advantage of increased signals and the reduced influence of artefacts, is the ability of detecting a bigger variety of anatomical structures in the brain based on their chemical signature (instead of just white *vs* grey matter). Figure 6-10 shows the result of image PCA on a brain tissue section in the hippocampus area, analysed frozen hydrated. The areas distinguished by PCA correspond to different brain structures which can be found in the Allen Developing Mouse Brain Atlas (dataset P56, sagittal),[182] as shown in Figure 6-10 (d). PCA also highlights signals only present in specific areas displayed in Figure 6-10 (e) and in the ToF-SIMS overlay image in Figure 6-12 (a) which shows the ganglioside species GM1 (38:1) at *m/z* 1572.9 is almost exclusively present in the

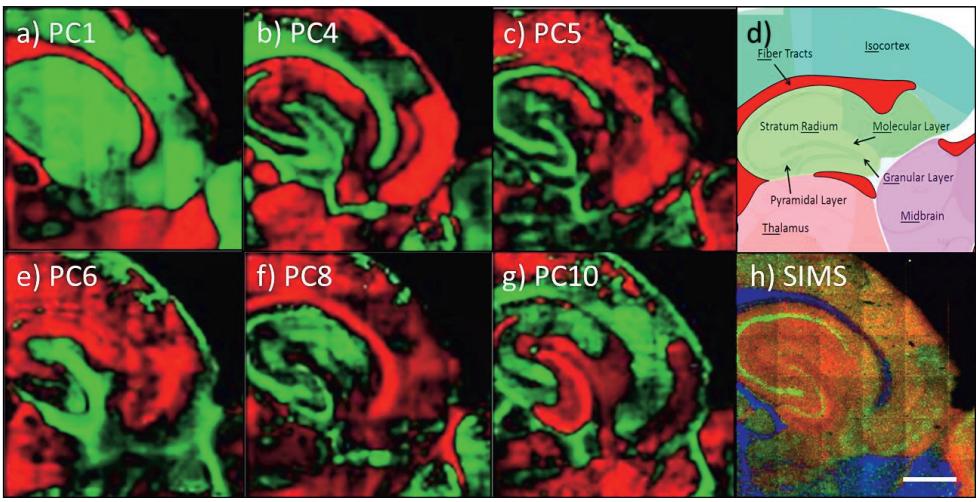

Figure 6-10 Results for image PCA performed on a frozen hydrated brain section, analysed by ToF-SIMS at a stable temperature of 100 K in negative ion mode. Shown are principal components a) 1, b) 4, c) 5, e) 6, f) 8 and g) 10 as these display greatest chemical variety in and around the hippocampal formation. Positive scoring pixels in each PC are displayed in green, negative scoring pixels in red. Pixels with little or no variation in each PC are black. d) Shows an image retrieved from the Allen Developing Mouse Brain Atlas, with manually added labels, that displays structures and assignments according to histology of the different brain regions that can be found in the PCA images. h) red/green/blue overlay ToF-SIMS image showing chemical variety in different brain regions, the peaks used to generate this image are *m/z* 766.53 PE(38:4) $[M-H]^-$, *m/z* 885.54 PI(38:4) $[M-H]^-$and *m/z* 906.63 Ch24:0 Sulfatide $[M-H]^-$. The white scale bar represents 1 mm. Reprinted with permission from T. B. Angerer, A. S. Mohammadi, J. S. Fletcher, *Biointerphases* 2016, 11, 02A319. Copyright 2016 American Vacuum Society.

outer molecular layer of dentate gyrus. Although frozen hydrated analysis is the best option, it is not always feasible to keep samples in this condition. Fortunately there are ways to restore already dried samples, for example *via* TFA and NH_3 treatment. The disadvantage of those treatments is that they partially restrict later analysis options.

6.3.7 Results: TFA (Paper IV)

TFA is a highly acidic and very volatile substance; therefore it should introduce additional positive changes (H^+, protons) into the tissue without building up on the surface/leaving the surface in vacuum. Also vapour should not lead to delocalisation of chemicals as would be the case for *e.g.* liquid droplets on the sample. The ideal timeframe with our set up was about 30 minutes exposure (cholesterol removed in white matter, lipid signals enhanced in grey matter and granular area). Shorter exposure (15 min.) did not remove cholesterol completely and longer exposure (60 min.) led to degradation of the tissue. The results from 30 minutes TFA exposure are shown in Figure 6-11. SEM images show that TFA removes cholesterol from the surface and uncovers the underlying signals. Additionally it acts as ionisation source for species which are only weak (Figure 6-11 (c), (d) *vs* (i), (j)) or not present (Figure 6-11 (e), (f) *vs* (k), (l)) during freeze dried brain analysis. Those additional signals highlight brains areas which are barely detectable in positive ion mode freeze dried analysis (displayed in green, granular layer in cerebellum Figure 6-11 (a) vs (b)). For negative ion mode analysis TFA exposure partially decreases signals, as expected but the advantages due to the removed

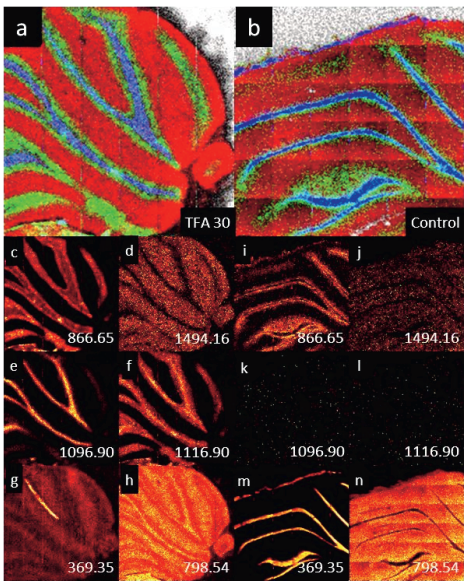

Figure 6-11 RGB overlays of a 30 minute TFA exposed rodent brain (a) and control brain (b) (red *m/z* 570.53, green *m/z* 866.65 and blue *m/z* 1096.90 for TFA and *m/z* 369.35 for the control section). Below is a comparison of single ion images for 30 minute TFA exposure (c - h), control brain (I - n) of *m/z* 886.65 (c + i), *m/z* 1494.16 (d + j), *m/z* 1096.90 (e + k), *m/z* 1116.90 (f + l), *m/z* 369.35 (g + m) and *m/z* 798.54 (h + n). Peak identities can be found in the peak list in Table 1. All data was acquired using 40 keV Ar_{4000}^+ primary ion dose density 7×10^{11} ions/cm^2 in positive ion mode. Image area of 4.8 × 4.8 mm^2 comprising 192 × 192 pixels. Reprinted with permission from T. B. Angerer, M. D. Pour, P. Malmberg, J. S. Fletcher, *Anal. Chem.* 2015, 87, 4305-4313. Copyright 2016 American Chemical Society

cholesterol remains. In conclusion: TFA is improving dried brain analysis in positive ion mode.

6.3.8 Results: NH_3 (Paper V)

NH_3 exposure of dried brain tissue has some effects similar to TFA exposure as it reduces cholesterol signal/ partially removes the crystals from the surface but a significant signal increase in negative ion mode was not observed after 60 minutes exposure. Tissue degradation was not observed either, so a harsher treatment (higher NH_3 concentrations or longer exposure times) could lead to more pronounced results. What was observed were lipid profiles and distributions closer to frozen hydrated analysis as shown in Figure 6-12. Especially the localisation of ganglioside signals, NH_3 treatment (c) shows a clear advantage over freeze drying (b) therefore the exposure enables better identification of anatomic structures within the hippocampus, based on their chemical signature.

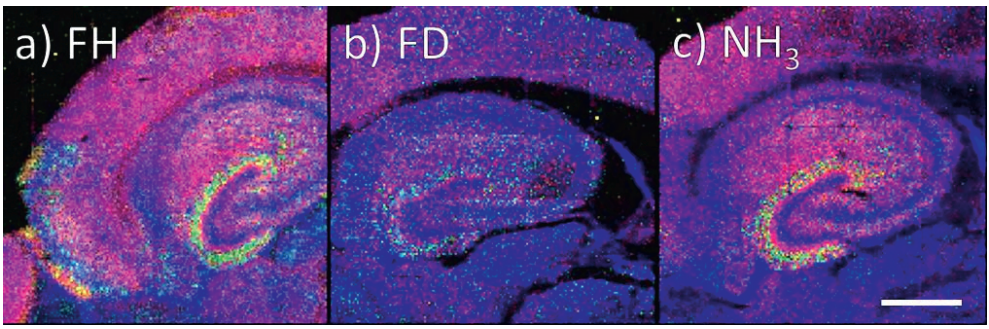

Figure 6-12 ToF-SIMS images comparing a) frozen hydrated (FH), b) freeze dried (FD) and c) ammonia treatment (NH_3) with focus on the isocortex and molecular layer brain areas. The peaks used to generate the red green blue overlay image are *m/z* 885.5 PI(38:4) $[M-H]^-$, *m/z* 1544.9 GM1 (36:1) $[M-H]^-$, *m/z* 1572.9 GM1 (38:1) $[M-H]^-$. The white scale bar represents 1 mm. All data was acquired using 40 keV Ar_{4000}^+, ion dose: 1×10^{12} ions/cm^2, negative ion mode. Reprinted with permission from T. B. Angerer, A. S. Mohammadi, J. S. Fletcher, *Biointerphases* 2016, 11, 02A319. Copyright 2016 American Vacuum Society.

6.3.9 Conclusion: Brain Sample Treatment

Although the novel GCIB technology is beneficial for brain analysis, the nature of the sample (soft, shrinking while drying, containing migrating species) poses challenges. For a life-like representation of the molecular composition of the brain in ToF-SIMS, frozen hydrated sample analysis is ideal while TFA exposure for positive ion mode and NH_3 for negative ion mode are valid options.

6.4 Breast Cancer: "A Picture is Worth a Thousand Words"

6.4.1 Overview

Due to improved detection and treatment techniques breast cancer mortality rates are at an all-time low (~90% 5 year survival in the US[183], numbers vary worldwide). This is good news but one has to consider that breast cancer is still the most occurring cancer and the worldwide leading cause of cancer related deaths in woman. Breast cancer is a heterogeneous disease with many subtypes, some of them very aggressive, as well as sub-populations of cells within one cancerous growth, that may or may not respond to treatment and can cause the cancer to reoccur.[184] To improve personalised treatments, studies of the cancerous microenvironment have become of increasing interest. Also, the significance of lipids for cancer development and progression has been recognised.

ToF-SIMS imaging has been used to good effect in a range of biomedical studies on human samples including prostate cancer,[185] colon cancer,[186] fatty liver,[187] atherosclerotic plaque,[188] adipose tissue,[189] skeletal muscle,[190] teeth[191] and recently breast cancer.[192] The combination with novel GCIB technology makes ToF-SIMS more sensitive to molecular signals and therefore well suited to study the cancerous lipid microenvironment. To realise the potential of this development a collaboration between our research facility and the Sahlgrenska Cancer Centre was formed. In a preliminary study 9 breast cancer sections with varying diagnosis were analysed and their lipid distributions in different parts of the tissue were studied.

Summary of results from this study:

- Stroma, cancer and necrotic areas (if present) showed clearly distinguishable molecular profiles, which were similar between all analysed sections.
- Previously presumed cancer markers (FA(20:4)) were shown to originate from inflammatory cells and are not connected to cancer fatty acid metabolism.
- Fatty acid distribution in and around tumorous growths indicates that all tumour fatty acids are *de novo* synthesised.
- Imaging PCA shows within tumour heterogeneity connected to fatty acid saturation changes.

6.4.2 Lipids in Cancer

Fatty acid and lipid metabolism in cancer cells has become of increased interest over the last 20 years.[193-194] Many studies focus on the influence of dietary fatty acid (FA) intake and the effects on cancer (*e.g.* ω3 versus ω6 FAs).[195] Although certain claims are made, the ultimate fate/involvement of those FAs on cancer occurrence and progression is unknown. For most cells dietary fatty acids are the main base component for the synthesis of structural and signalling lipids but this is not necessarily the case for cancer cells. The enzyme fatty acid synthase (FASN) has been shown to be upregulated in many cancer types and is usually linked to a poor prognosis.[193] FASN is the major enzyme responsible for *de novo* fatty acid synthesis in mammalian cells. In a healthy organism it is mainly active to transform an overabundance of nutrients into FAs which are eventually bound in triacylglycerides (TAGs), so called storage fat, and during lactation in mammary glands.[196] The storage fat can be an energy resource as it is broken down *via* β-oxidation during starvation or exercise. Cancer cells are not known to produce storage fat, therefore there has to be another explanation for this increased FASN activity. This in combination with the high glucose uptake of cancer cells[197] make it plausible that cancer cells *de-novo* synthesise their own fatty acids, rather than relying on dietary sources. FASN is currently under investigation as a therapeutic target but tested inhibitors show severe side effects.[198]

6.4.3 Summary of Methods

Cancer sections were frozen in liquid nitrogen immediately after surgery and kept at -80 °C until cryo-sectioning at 12 µm thickness under argon, thaw mounted on to ITO-glass and dried in vacuum. Sections were then analysed with the Ionoptika J105 using 40 keV Ar_{4000}^{+} with different image resolutions and primary ion currents. Imaging PCA in MatLab (The MathWorks Inc.) and spectral PCA in SIMCA (Umetrix, Sweden) was performed on the data.

6.4.4 Results: Breast Cancer (Paper VI)

Figure 6-13 shows a high resolution H&E stain image of cancer section #9 included in paper VI[6] as well as several analysed areas in positive and negative ion mode as they highlight all our major findings. The fatty acid FA(20:4) and connected lipid species PI(38:4) are almost exclusively detected outside the cancerous areas (red, (B), (E) and (H)), while the potentially *de-novo* synthesised species FA(20:3), FA(20:2) and connected lipid species PI(38:3), PI(38:2) are

mainly found within the cancerous areas. Higher resolution MS images show that FA(20:4)/PI(38:4) signals co-localise with the inflammatory cells in the tissue (E). This explains, why FA(20:4) was previously correlated with cancer, as the inflammatory cells are present in higher amounts in breast tissue with cancer than in healthy tissue and the experiments that led to this conclusion (FA20:4 being related to cancer cells) were performed on homogenised tissue.[199] Location specific information reveals that FA(20:4) is not correlated with cancer fatty acid metabolism as previously assumed.

FA(20:3) and FA(20:2) signals are not evenly distributed in the cancerous tissue. Some areas are dominated by FA(20:3)/PI(30:3), displayed in green and some by FA(20:2)/PI((38:2) in blue in (B), (E), (H). In general, the blue areas are dominated by saturated and monounsaturated fatty acids while the green areas mainly contain polyunsaturated fatty acids. Those areas are not distinguishable in H&E stains. The variations in saturation could occur due to oxygen availability differences but the distribution does not support this theory, as we would expect the blue areas in the centre, surrounded by the green areas. Another explanation could be that the saturation differences are part of the cancer cell programming, as unsaturated lipid membranes increase membrane fluidity, necessary for dividing and invading cells. Membranes with higher degrees of saturation have been connected with lower drug permeability.[200] Those cells could form the persistent core of the cancerous growth, less effected by chemotherapy. Evidence that these characteristics are specific for cancer and do not in apply to epithelial cells (the precursor for breast cancer cells) is shown in (I) and (J). (I) shows a hyperplasia duct, a milk duct with degenerated cells, considered potentially pre-cancerous, and (J) a normal milk duct. While FA(20:3) is elevated in the hyperplasia duct, the normal milk duct shows no signs of this fatty acid, but has a fatty acid distribution closer to the inflammatory cells. In positive ion mode the differences between cancerous and stroma areas are less pronounced as displayed in (C) and (F) but observable trends are: PC(32:0) and fat-storage species (DAGs, TAGs) are mainly outside the cancerous areas; PC(34:1) is more strongly detected in the cancerous growths.

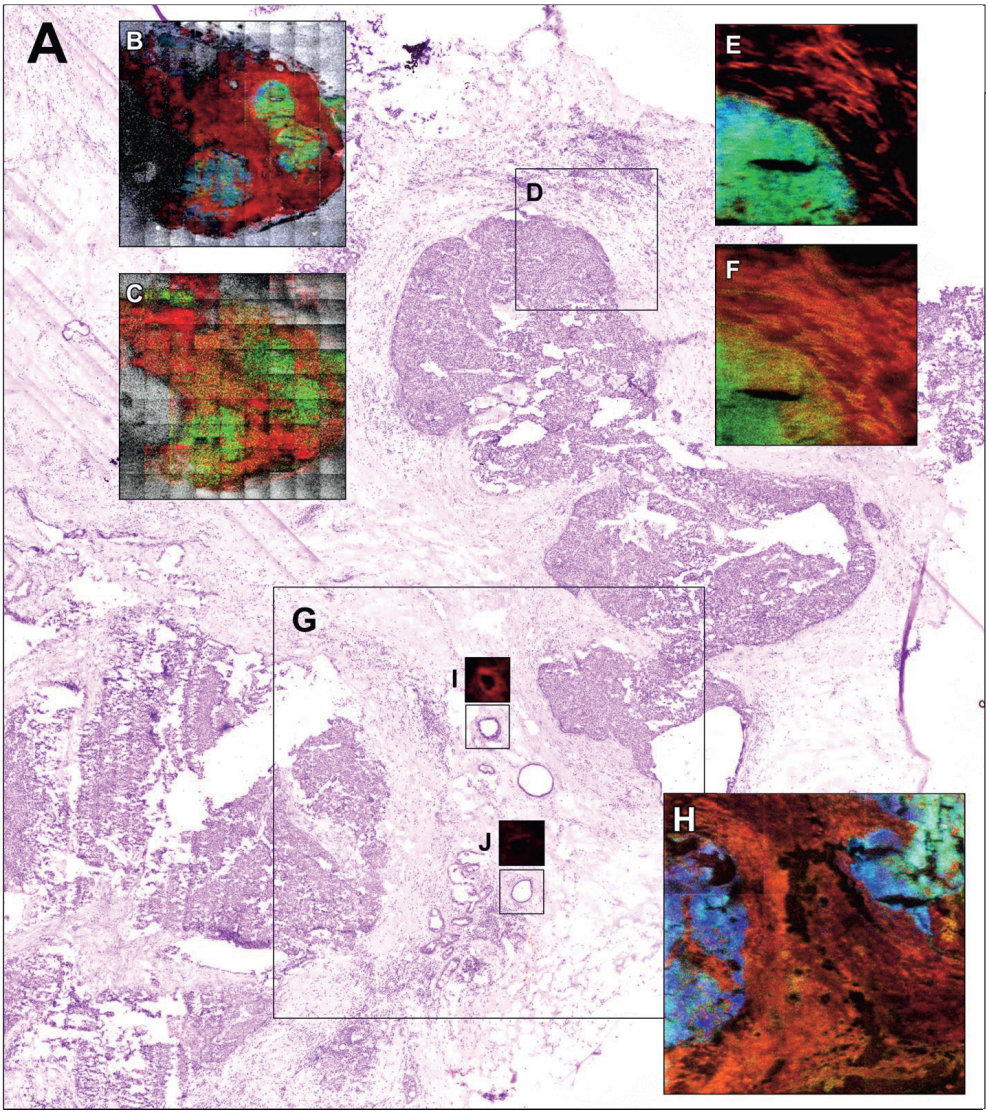

Figure 6-13 (A) H&E stained microscopy image of a tissue section consecutive to MS-analysed section, showing cancerous (purple) and stroma (bright) tissue, (B) MS RGB overlay image in negative ion mode of the whole tissue section, showing lipid species PI(38:4), PI(38:3), and PI(38:2), image size 9 mm, 31.25 µm/pixel; (C) MS RG overlay image in positive ion mode of the whole tissue section, showing lipid species PC(34:1)+H and +K, PC(32:0)+Na and DAG(36:2)–H_2O, image size 9mm, 31.25 µm/pixel; (D) Part of the tissue displayed in MS images E and F; (E) MS RGB overlay image in negative ion mode, same lipid species as B, image size 1 mm, 3.9 µm/pixel; (F) MS RG overlay image in positive ion mode, same lipid species as C, image size 1 mm, 3.9 µm/pixel; (G) Part of the tissue displayed in MS image H; (H) MS RGB overlay image in negative ion mode, showing fatty acid species FA(20:4), FA(20:3), and FA(20:2), image size 3 mm, 7.8 µm/pixel; (I/J) Dual ion images (FA(20:3) + FA(20:2)) of (I) hyperplasia duct and (J) normal milk duct.

6.4.5 Conclusions: Breast Cancer Lipid Heterogeneity

The new evidence presented by this work fits with previously reported data, as well as explaining previous misconceptions by providing cellular, location specific information and high chemical coverage and specificity. There is evidence that the majority of fatty acids in cancer cell membranes are *de-novo* synthesised, supported by the fact that the enzyme fatty acid synthase is upregulated in cancer cells and the discovered fatty acid species found in cancerous areas correlate with *de-novo* synthesis pathways, while essential fatty acids are correlated with inflammatory cells outside the cancerous tissue. We theorise that within cancer lipid heterogeneity could be connected to diverse cell behaviour and treatment responses but additional research is necessary to confirm this theory and elucidate the mechanisms behind it.

7 Concluding Remarks

In this thesis imaging ToF-SIMS has been shown to be capable of imaging small structures within in cells in 2D and 3D while also monitoring lipid membrane changes on a cellular scale. New ion beam technology has brought SIMS closer to the MALDI regime by enhancing its capability to image larger secondary ions (>1500 Da) and improved sample treatment is generating a more life-like representation of lipids in ToF-SIMS images of brain tissue. Lastly, it has been shown that from ToF-SIMS results, conclusions about disease related, altered lipid metabolism can be drawn.

ToF-SIMS imaging is a powerful and versatile technique but there are still issues (surface charging, ionisation efficiency differences, matrix effects, fragmentation, beam focus and secondary ion yields) that need to be addressed and offer scope for improvement.

Ultimately no one technique can answer all of sciences questions but with multimodal approaches and constant technological improvements and innovations and the sharing of discoveries we can expand our knowledge to one day make the issues of today, problems of the past.

Acknowledgements

I want to thank my lab mates, all of you, for providing help during projects, for training me up in the beginning, for scientific discussion, all the insights into different cultures and the goofy fun we had during the time we were supposed to work, and after. Thank you for coping with me. I loved being here those last 4.5 years, you made my world bigger.

I thank my supervisor John for all the support and help I got in oh so many ways, be it science related, lots of science, carrying around my conferences cloths between continents or providing me with some extra motivation (Pink Drinks! Yeah!).

Also thanks to his wife, Lorna for giving me the first hug when I arrived.

Thanks to my second supervisor Andy for next to unlimited resources and providing this awesome setup and environment to do science in.

Big thanks to the nice ladies from the administration, who were always eager to help and found a solution to my problems 95%±2 of the time.

Thanks to my favourite Skype friends from Ionoptika, Paul and Gavyn who taught me that there's nothing you cannot do with instrument schematics, a little webcam, a bad internet connection and a screwdriver.

Thank you, Jenny and Alex. You made me feel truly integrated into Swedish society so that I'm not just working here, I'm living here too.

Thank you, my oldest friend Sarah for WhatsApp counselling, amazing breakfasts, drinks in the pool and 20 years of friendship.

To my second family, the Lundhs, I came into your house and you took my into your heart with no ifs or buts and no holding back.

Thank you, YouTube, Google and Wikipedia, without you I would not have gotten my degrees.

Espressohouse, where I wrote my thesis, set there for 8h, using your free WiFi, buying a small coffee and getting at least 5 refills.

To my husband, thank you for taking me unconditionally as the smartass, chubby, weird, strange phobia riddled, stubborn, notorious piece of love that I am and following me to hell and back. I love you!

And last but not least, my mum, bent but never broken, the strongest person in the universe. Because of you I know, wherever I go, whatever I do, you'll support me and that's why it's going to be okay. Thank You.

Appendix

8 Abstracts from Additional Papers:

8.1 Paper (S) I

Maximising the potential for bacterial phenotyping using time-of-flight secondary ion mass spectrometry with multivariate analysis and Tandem Mass Spectrometry[7]

Authors: Patrick M. Wehrli, Erika Lindberg, Tina B. Angerer, Agnes E. Wold, Johan Gottfries, John S. Fletcher

Abstract: The increasing trend towards bacteria becoming resistant to current antibiotic treatments is of great concern to the healthcare industry with severe potential consequences for society as a whole. In many cases, it is the interaction of the antibacterial agent with the targets within the bacterial envelope of the microorganism that is a critical factor. Time-of-flight secondary ion mass spectrometry (ToF-SIMS) is uniquely capable of probing the chemistry in this region. This study aimed at optimising sample preparation and data pre-processing for bacterial analysis with ToF-SIMS and principal components analysis to study small chemical differences related to changes in bacterial phenotype that will help to find new antibiotics and understand how antibiotics are trafficked in the bacteria. ToF-SIMS analysis was performed using a J105 instrument equipped with a 40 kV C_{60}^+ion source. Combination of positive and negative ion mode data enhanced the multivariate model quality regarding classification and aided chemical identification particularly when coupled with tandem mass spectrometry.

Contribution: Optimising sample preparation and analysis conditions for and performing ToF-SIMS analysis on bacteria samples.

8.2 Paper (S) II

Analysis of liposome model systems by time-of-flight secondary ion mass spectrometry[8]

Authors: Jelena Lovrić, Jacqueline D. Keighron, Tina B. Angerer, Xianchan Li, Per Malmberg, John S. Fletcher, Andrew G. Ewing

Abstract: Time-of-flight secondary ion mass spectrometry (ToF-SIMS) is an important technique for studying chemical composition of micrometer scale objects because of its high spatial resolution imaging capabilities and chemical specificity. In this work, we focus on the application of ToF-SIMS to gain insight into the chemistry of micrometer size liposomes as a potential model for neurotransmitter vesicles. Two models of giant liposomes were analyzed: histamine and aqueous two-phase system-containing liposomes. Characterization of the internal structure of single fixed liposomes was carried out both with the Bi_3^+ and C_{60}^+ ion sources. The depth profiling capability of ToF-SIMS was used to investigate the liposome interior.

Contribution: Performing ToF-SIMS analysis on differently prepared liposome samples, generating figures and assisting with spectra interpretation.

8.3 Paper (S) III

Significant Enhancement of Negative Secondary Ion Yields by Cluster Ion Bombardment Combined with Cesium Flooding[9]

Authours: Patrick Philipp, Tina B. Angerer, Sanna Sämfors, Paul Blenkinsopp, John S. Fletcher, and Tom Wirtz

Abstract: In secondary ion mass spectrometry (SIMS), the beneficial effect of cesium implantation or flooding on the enhancement of negative secondary ion yields has been investigated in detail for various semiconductor and metal samples. All results have been obtained for monatomic ion bombardment. Recent progress in SIMS is based to a large extent on the development and use of cluster primary ions. In this work we show that the enhancement of negative secondary ions induced by the combination of ion bombardment with simultaneous cesium flooding is valid not only for monatomic ion bombardment but also for cluster primary ions. Experiments carried out using C_{60}^+ and Ar_{4000}^+ bombardment on silicon show that yields of negative secondary silicon ions can be optimized in the same way as by Ga^+ and Cs^+ bombardment. Both for monatomic and cluster ion bombardment, the optimization does not depend on the primary ion species. Hence, it can be assumed that the silicon results are also valid for other cluster primary ions and that results obtained for monatomic ion bombardment on other semiconductor and metal samples are also valid for cluster ion bombardment. In SIMS, cluster primary ions are also largely used for the analysis of organic matter. For polycarbonate, our results show that Ar_{4000}^+ bombardment combined with cesium flooding enhances secondary ion signals by a factor of 6. This can be attributed to the removal of charging effects and/or reduced fragmentation, but no major influence on ionisation processes can be observed. The use of cesium flooding for the imaging of cells was also investigated and a significant enhancement of secondary ion yields was observed. Hence, cesium flooding has also a vast potential for SIMS analyses with cluster ion bombardment

Contribution: Analysing silicon and polymer samples with ToF-SIMS with different amounts of Cs, generating depth-profiles, interpreting spectra, identifying fragments and generating figures.

8.4 Paper (S) IV

Cholesterol Alters the Dynamics of Release in Protein Independent Cell Models for Exocytosis[10]

Authors: Neda Najafinobar, Lisa J. Mellander, Michael E. Kurczy, Johan Dunevall, Tina B. Angerer, John S. Fletcher, and Ann-Sofie Cans

Abstract: Neurons communicate *via* an essential process called exocytosis. Cholesterol, an abundant lipid in both secretory vesicles and cell plasma membrane can affect this process. In this study, amperometric recordings of vesicular dopamine release from two different artificial cell models created from a giant unilamellar liposome and a bleb cell plasma membrane, show that with higher membrane cholesterol the kinetics for vesicular release are decelerated in a concentration dependent manner. This reduction in exocytotic speed was consistent for two observed modes of exocytosis, full and partial release. Partial release events, which only occurred in the bleb cell model due to the higher tension in the system, exhibited amperometric spikes with three distinct shapes. In addition to the classic transient, some spikes displayed a current ramp or plateau following the maximum peak current. These post spike features represent neurotransmitter release from a dilated pore before constriction and show that enhancing membrane rigidity *via* cholesterol adds resistance to a dilated pore to re-close. This implies that the cholesterol dependent biophysical properties of the membrane directly affect the exocytosis kinetics and that membrane tension along with membrane rigidity can influence the fusion pore dynamics and stabilization which is central to regulation of neurochemical release.

Contribution: Analysing frozen hydrated cells with ToF-SIMS to measure enhanced cholesterol content in the outer cell membrane, generating the figure, writing SIMS related parts of the manuscript.

8.5 Paper (S) V

Investigating the Role of the Stringent Response in Lipid Modifications during the Stationary Phase in E. coli by Direct Analysis with Time-of-Flight-Secondary Ion Mass Spectrometry[11]

Authors: Patrick M. Wehrli, Tina B. Angerer, Anne Farewell, John S. Fletcher, and Johan Gottfries

Abstract: Escherichia coli is able to rapidly adjust the biophysical properties of its membrane phospholipids to adapt to environmental challenges including starvation stress. These membrane lipid modifications were investigated in glucose starved E. coli cultures and compared to a Δ*rel*AΔ*spo*T (ppGpp^0) mutant strain of E. coli, deficient in the stringent response, by means of time-of-flight-secondary ion mass spectrometry (TOF-SIMS). Recent advances in TOF-SIMS, through the implementation of gas cluster ion beams (GCIBs), now permit the analysis of higher mass species from native, underivatized, biological specimen, i.e., intact bacterial cells. Cultures in stationary phase were found to exhibit a radically different lipid composition as compared to cultures in the exponential growth phase. Wild-type E. coli reacted upon carbon starvation by lipid modifications including elongation, cyclopropanation, and increased cardiolipin formation. Observations are consistent with variants of cardiolipins (CL), phosphatidylglycerols (PG), phosphatidylethanolamines (PE), phosphatidic acids (PA), and fatty acids. Notably, despite having a proteomic profile and a gene expression profile somewhat similar to the wild-type during growth, the ppGpp^0 mutant E. coli strain was found to exhibit modified phospholipids corresponding to unsaturated analogues of those found in the wild-type. We concluded that the ppGpp^0 mutant reacts upon starvation stress by elongation and desaturation of fatty acyl chains, implying that only the last step of the lipid modification, the cyclopropanation, is under stringent control. These observations suggest alternative stress response mechanisms and illustrate the role of the RelA and SpoT enzymes in the biosynthetic pathway underlying these lipid modifications.

Contribution: Optimising conditions for and performing ToF-SIMS analysis on bacteria samples.

References

[1] T. B. Angerer, J. S. Fletcher, *Surf Interface Anal* **2014**, *46*, 198-203.
[2] T. B. Angerer, P. Blenkinsopp, J. S. Fletcher, *Int J Mass Spectrom* **2015**, *377*, 591-598.
[3] A. G. Shard, R. Havelund, S. J. Spencer, I. S. Gilmore, M. R. Alexander, T. B. Angerer, S. Aoyagi, J. P. Barnes, A. Benayad, A. Bernasik, G. Ceccone, J. D. P. Counsell, C. Deeks, J. S. Fletcher, D. J. Graham, C. Heuser, T. G. Lee, C. Marie, M. M. Marzec, G. Mishra, D. Rading, O. Renault, D. J. Scurr, H. K. Shon, V. Spampinato, H. Tian, F. Y. Wang, N. Winograd, K. Wu, A. Wucher, Y. F. Zhou, Z. H. Zhu, V. Cristaudo, C. Poleunis, *J Phys Chem B* **2015**, *119*, 14337-14337.
[4] T. B. Angerer, M. D. Pour, P. Malmberg, J. S. Fletcher, *Anal Chem* **2015**, *87*, 4305-4313.
[5] T. B. Angerer, A. S. Mohammadi, J. S. Fletcher, *Biointerphases* **2016**, *11*, 02A319.
[6] T. B. Angerer, Y. Magnusson, G. Landberg, J. S. Fletcher, *Anal Chem* **2016**, *88*, 11946-11954.
[7] P. M. Wehrli, E. Lindberg, T. B. Angerer, A. E. Wold, J. Gottfries, J. S. Fletcher, *Surf Interface Anal* **2014**, *46*, 173-176.
[8] J. Lovric, J. D. Keighron, T. B. Angerer, X. C. Li, P. Malmberg, J. S. Fletcher, A. G. Ewing, *Surf Interface Anal* **2014**, *46*, 74-78.
[9] P. Philipp, T. B. Angerer, S. Samfors, P. Blenkinsopp, J. S. Fletcher, T. Wirtz, *Anal Chem* **2015**, *87*, 10025-10032.
[10] N. Najafinobar, L. J. Mellander, M. E. Kurczy, J. Dunevall, T. B. Angerer, J. S. Fletcher, A. S. Cans, *Sci Rep-Uk* **2016**, *6*.
[11] P. M. Wehrli, T. B. Angerer, A. Farewell, J. S. Fletcher, J. Gottfries, *Anal Chem* **2016**, *88*, 8680-8688.
[12] B. Alberts, A. Johnson, J. Lewis, e. al., *Molecular Biology of the Cell. The Lipid Bilayer.*, 4 ed., Garland Science, New York, **2002**.
[13] E. Fahy, S. Subramaniam, R. C. Murphy, M. Nishijima, C. R. H. Raetz, T. Shimizu, F. Spener, G. van Meer, M. J. O. Wakelam, E. A. Dennis, *J Lipid Res* **2009**, *50*, S9-S14.
[14] J. M. Berg, J. L. Tymoczko, L. Stryer, *Biochemistry, Chapter 12*, 5 ed., W H Freeman, New York, **2002**.
[15] M. M. Or-Rashid, N. E. Odongo, B. W. McBride, *J Anim Sci* **2007**, *85*, 1228-1234.
[16] E. Christiansen, S. Schnider, B. Palmvig, E. TauberLassen, O. Pedersen, *Diabetes Care* **1997**, *20*, 881-887.
[17] B. C. Davidson, R. C. Cantrill, *S Afr Med J* **1985**, *67*, 633-634.
[18] A. D. McNaught, A. Wilkinson, *I{UPAC}. Compendium of Chemical Terminology, 2nd ed. (the "Gold Book")*, WileyBlackwell; 2nd Revised edition edition.
[19] J. E. Vance, R. Steenbergen, *Prog Lipid Res* **2005**, *44*, 207-234.
[20] A. Lehninger, D. Nelson, M. Cox, *Lehninger Principles of Biochemistry*, W. H. Freeman, **2008**.
[21] E. P. Kennedy, S. B. Weiss, *J Biol Chem* **1956**, *222*, 193-213.
[22] F. Gibellini, T. K. Smith, *Iubmb Life* **2010**, *62*, 414-428.
[23] R. Weigert, M. G. Silletta, S. Spano, G. Turacchio, C. Cericola, A. Colanzi, S. Senatore, R. Mancini, E. V. Polishchuk, M. Salmona, F. Facchiano, K. N. J. Burger, A. Mironov, A. Luini, D. Corda, *Nature* **1999**, *402*, 429-433.
[24] R. J. King, M. C. Macbeth, *Biochimica Et Biophysica Acta* **1981**, *647*, 159-168.
[25] R. Wood, R. D. Harlow, *Arch Biochem Biophys* **1969**, *131*, 495-&.
[26] D. Shields, P. Arvan, *Curr Opin Cell Biol* **1999**, *11*, 489-494.

[27] N. Divecha, R. F. Irvine, *Cell* **1995**, *80*, 269-278.
[28] A. Saiardi, H. Erdjument-Bromage, A. M. Snowman, P. Tempst, S. H. Snyder, *Curr Biol* **1999**, *9*, 1323-1326.
[29] M. P. Czech, *Cell* **2000**, *100*, 603-606.
[30] M. L. Greenberg, J. M. Lopes, *Microbiol Rev* **1996**, *60*, 1-&.
[31] L. C. Foukas, I. M. Berenjeno, A. Gray, A. Khwaja, B. Vanhaesebroeck, *P Natl Acad Sci USA* **2010**, *107*, 11381-11386.
[32] W. Dowhan, *Annu Rev Biochem* **1997**, *66*, 199-232.
[33] J. E. Vance, *J Lipid Res* **2008**, *49*, 1377-1387.
[34] F. Furt, P. Moreau, *Int J Biochem Cell B* **2009**, *41*, 1828-1836.
[35] M. Bogdanov, J. Xie, P. Heacock, W. Dowhan, *J Cell Biol* **2008**, *182*, 925-935.
[36] A. Momchilova, T. Markovska, *Int J Biochem Cell B* **1999**, *31*, 311-318.
[37] A. Sune, P. Bette-Bobillo, A. Bienvenue, P. Fellmann, P. F. Devaux, *Biochemistry* **1987**, *26*, 2972-2978.
[38] B. Verhoven, R. A. Schlegel, P. Williamson, *The Journal of Experimental Medicine* **1995**, *182*, 1597-1601.
[39] R. F. A. Zwaal, P. Comfurius, E. M. Bevers, *Biochimica et Biophysica Acta (BBA) - Reviews on Biomembranes* **1998**, *1376*, 433-453.
[40] J. K. Blusztajn, M. Liscovitch, U. I. Richardson, *P Natl Acad Sci USA* **1987**, *84*, 5474-5477.
[41] L. K. Cole, J. E. Vance, D. E. Vance, *Bba-Mol Cell Biol L* **2012**, *1821*, 754-761.
[42] LHcheM, Wikipedia, **2012**.
[43] C. R. Gault, L. M. Obeid, Y. A. Hannun, *Adv Exp Med Biol* **2010**, *688*, 1-23.
[44] J. P. Jaffrezou, T. Levade, A. Bettaieb, N. Andrieu, C. Bezombes, N. Maestre, S. Vermeersch, A. Rousse, G. Laurent, *Embo J* **1996**, *15*, 2417-2424.
[45] F. W. McLafferty, F. Tureček, *Interpretation of Mass Spectra*, University Science Books, **1993**.
[46] I. Ishizuka, *Prog Lipid Res* **1997**, *36*, 245-319.
[47] J. Marcus, S. Honigbaum, S. Shroff, K. Honke, J. Rosenbluth, J. L. Dupree, *Glia* **2006**, *53*, 372-381.
[48] T. Takahashi, T. Suzuki, *J Lipid Res* **2012**, *53*, 1437-1450.
[49] R. G. Parton, *J Histochem Cytochem* **1994**, *42*, 155-166.
[50] R. K. Yu, Y. T. Tsai, T. Ariga, M. Yanagisawa, *J Oleo Sci* **2011**, *60*, 537-544.
[51] M. Bloom, O. G. Mouritsen, *Can J Chem* **1988**, *66*, 706-712.
[52] K. E. Bloch, *Crc Cr Rev Bioch Mol* **1979**, *7*, 1-5.
[53] J. F. Frisz, H. A. Klitzing, K. Lou, I. D. Hutcheon, P. K. Weber, J. Zimmerberg, M. L. Kraft, *Journal of Biological Chemistry* **2013**, *288*, 16855-16861.
[54] D. S. Millington, N. Kodo, D. L. Norwood, C. R. Roe, *J Inherit Metab Dis* **1990**, *13*, 321-324.
[55] G. Siuzdak, **2016**.
[56] J. J. Thomson, *Phil Mag Lett* **1897**, *44*, 293 - 316.
[57] F. W. Aston, *Nature* **1920**, *105*, 617-619.
[58] A. O. Nier, *Phys Rev* **1939**, *55*, 0150-0153.
[59] A. O. Nier, E. A. Gulbransen, *J Am Chem Soc* **1939**, *61*, 697-698.
[60] W. E. Stephens, *Phys Rev* **1946**, *69*, 691-691.

[61] B. A. Mamyrin, V. I. Karataev, D. V. Shmikk, V. A. Zagulin, *Zh Eksp Teor Fiz+* **1973**, *64*, 82-89.
[62] Comisaro.Mb, A. G. Marshall, *Chem Phys Lett* **1974**, *25*, 282-283.
[63] R. E. Honig, *J Appl Phys* **1958**, *29*, 549-555.
[64] Benningh.A, *Phys Status Solidi* **1969**, *34*, K169-&.
[65] K. Biemann, J. Seibl, F. Gapp, *Biochem Bioph Res Co* **1959**, *1*, 307-311.
[66] M. S. B. Munson, F. H. Field, *J Am Chem Soc* **1966**, *88*, 2621-&.
[67] M. Barber, R. S. Bordoli, R. D. Sedgwick, A. N. Tyler, *Nature* **1981**, *293*, 270-275.
[68] M. Karas, D. Bachmann, F. Hillenkamp, *Anal Chem* **1985**, *57*, 2935-2939.
[69] L. P. Verbit, *Appl Optics* **1983**, *22*, 2761-2761.
[70] N. Davies, D. E. Weibel, P. Blenkinsopp, N. Lockyer, R. Hill, J. C. Vickerman, *Appl Surf Sci* **2003**, *203*, 223-227.
[71] D. Touboul, F. Kollmer, E. Niehuis, A. Brunelle, O. Laprevote, *J Am Soc Mass Spectr* **2005**, *16*, 1608-1618.
[72] G. Gillen, S. Roberson, *Rapid Commun Mass Sp* **1998**, *12*, 1303-1312.
[73] S. C. C. Wong, R. Hill, P. Blenkinsopp, N. P. Lockyer, D. E. Weibel, J. C. Vickerman, *Appl Surf Sci* **2003**, *203*, 219-222.
[74] D. Weibel, S. Wong, N. Lockyer, P. Blenkinsopp, R. Hill, J. C. Vickerman, *Anal Chem* **2003**, *75*, 1754-1764.
[75] E. A. Jones, J. S. Fletcher, C. E. Thompson, D. A. Jackson, N. P. Lockyer, J. C. Vickerman, *Appl Surf Sci* **2006**, *252*, 6844-6854.
[76] E. A. Jones, N. P. Lockyer, J. C. Vickerman, *Int J Mass Spectrom* **2007**, *260*, 146-157.
[77] J. S. Fletcher, X. A. Conlan, E. A. Jones, G. Biddulph, N. P. Lockyer, J. C. Vickerman, *Anal Chem* **2006**, *78*, 1827-1831.
[78] A. G. Shard, F. M. Green, P. J. Brewer, M. P. Seah, I. S. Gilmore, *J Phys Chem B* **2008**, *112*, 2596-2605.
[79] J. S. Fletcher, N. P. Lockyer, S. Vaidyanathan, J. C. Vickerman, *Anal Chem* **2007**, *79*, 2199-2206.
[80] S. Ninomiya, K. Ichiki, H. Yamada, Y. Nakata, T. Seki, T. Aoki, J. Matsuo, *Rapid Commun Mass Sp* **2009**, *23*, 1601-1606.
[81] S. Rabbani, A. M. Barber, J. S. Fletcher, N. P. Lockyer, J. C. Vickerman, *Anal. Chem.* **2011**, *83*, 3793-3800.
[82] I. Yamada, J. Matsuo, N. Toyoda, A. Kirkpatrick, *Mat Sci Eng R* **2001**, *34*, 231-295.
[83] K. Mochiji, M. Hashinokuchi, K. Moritani, N. Toyoda, *Rapid Commun Mass Sp* **2009**, *23*, 648-652.
[84] R. F. K. Herzog, F. P. Viehbock, *Phys Rev* **1949**, *76*, 855-856.
[85] R. Castaing, G. Slodzian, *Cr Hebd Acad Sci* **1962**, *255*, 1893-&.
[86] H. Liebl, *J Appl Phys* **1967**, *38*, 5277-5283.
[87] R. M. Caprioli, T. B. Farmer, J. Gile, *Anal Chem* **1997**, *69*, 4751-4760.
[88] Z. Takats, J. M. Wiseman, B. Gologan, R. G. Cooks, *Science* **2004**, *306*, 471-473.
[89] J. Balog, L. Sasi-Szabo, J. Kinross, M. R. Lewis, L. J. Muirhead, K. Veselkov, R. Mirnezami, B. Dezso, L. Damjanovich, A. Darzi, J. K. Nicholson, Z. Takats, *Sci Transl Med* **2013**, *5*.
[90] T. Satoh, T. Sato, J. Tamura, *J Am Soc Mass Spectr* **2007**, *18*, 1318-1323.
[91] F. M. Green, I. S. Gilmore, M. P. Seah, *J Am Soc Mass Spectr* **2006**, *17*, 514-523.

[92] J. S. Fletcher, S. Rabbani, A. M. Barber, N. P. Lockyer, J. C. Vickerman, *Surf Interface Anal* **2013**, *45*, 273-276.
[93] J. Bailey, R. Havelund, A. G. Shard, I. S. Gilmore, M. R. Alexander, J. S. Sharp, D. J. Scurr, *ACS Applied Materials & Interfaces* **2015**, *7*, 2654-2659.
[94] D. Breitenstein, C. E. Rommel, R. Mollers, J. Wegener, B. Hagenhoff, *Angew Chem Int Edit* **2007**, *46*, 5332-5335.
[95] S. Jung, M. Foston, U. C. Kalluri, G. A. Tuskan, A. J. Ragauskas, *Angew Chem Int Edit* **2012**, *51*, 12005-12008.
[96] N. Matsunami, Y. Yamamura, Y. Itikawa, N. Itoh, Y. Kazumata, S. Miyagawa, K. Morita, R. Shimizu, H. Tawara, *Atomic Data and Nuclear Data Tables* **1984**, *31*, 1-80.
[97] J. C. Vickerman, D. Briggs, *TOF-SIMS: Materials Analysis by Mass Spectrometry*, SurfaceSpectra/IM Publications, **2013**.
[98] N. Laegreid, G. K. Wehner, *J Appl Phys* **1961**, *32*, 365-&.
[99] J. Kozole, N. Winograd, *Appl Surf Sci* **2008**, *255*, 886-889.
[100] H. Gnaser, K. Ichiki, J. Matsuo, *Rapid Commun Mass Sp* **2012**, *26*, 1-8.
[101] T. Seki, T. Murase, J. Matsuo, *Nucl Instrum Meth B* **2006**, *242*, 179-181.
[102] Z. Postawa, B. Czerwinski, M. Szewczyk, E. J. Smiley, N. Winograd, B. J. Garrison, *Anal Chem* **2003**, *75*, 4402-4407.
[103] A. Kramida, Ralchenko, Yu., Reader, J., and NIST ASD Team, National Institute of Standards and Technology, Gaithersburg, MD., Online, **2015**.
[104] Sponk, Wikipedia, **2013**.
[105] T. E. Conners, S. Banerjee, *Surface Analysis of Paper*, Taylor & Francis, **1995**.
[106] H. A. Storms, K. F. Brown, J. D. Stein, *Anal Chem* **1977**, *49*, 2023-2030.
[107] R. H. Sloane, R. Press, *Proc R Soc Lon Ser-A* **1938**, *168*, 284-301.
[108] C. A. Andersen, Hinthorn.Jr, *Science* **1972**, *175*, 853-&.
[109] T. Wirtz, H. N. Migeon, *Appl Surf Sci* **2004**, *231*, 940-944.
[110] A. Moser, K. Range, D. M. York, *Journal of Physical Chemistry B* **2010**, *114*, 13911-13921.
[111] E. R. A. van Hove, D. F. Smith, R. M. A. Heeren, *J Chromatogr A* **2010**, *1217*, 3946-3954.
[112] D. P. W. U. S. F. Professor, *Minds behind the Brain : A History of the Pioneers and Their Discoveries: A History of the Pioneers and Their Discoveries*, Oxford University Press, USA, **2000**.
[113] E. Abbe, *Journal of the Royal Microscopical Society* **1883**, *3*, 790-812.
[114] G. Sridharan, A. A. Shankar, *Journal of Oral and Maxillofacial Pathology : JOMFP* **2012**, *16*, 251-255.
[115] L. G. Luna, A. F. I. o. Pathology, *Manual of Histologic Staining Methods ; of the Armed Forces Institute of Pathology. Edited by Lee G. Luna*, Blakiston Division, McGraw-Hill, **1968**.
[116] G. Clark, H. Conn, *Staining procedures used by the Biological Stain Commission*, Published for the Biological Stain Commission by Williams & Wilkins, **1973**.
[117] L. De Broglie, Migration - université en cours d'affectation **1924**.
[118] J. J. Bozzola, L. D. Russell, *Electron Microscopy: Principles and Techniques for Biologists*, Jones and Bartlett, **1999**.
[119] E. Johnson, E. Seiradake, E. Y. Jones, I. Davis, K. Grünewald, R. Kaufmann, *Sci Rep-Uk* **2015**, *5*, 9583.

[120] A. M. Sydor, K. J. Czymmek, E. M. Puchner, V. Mennella, *Trends Cell Biol* **2015**, *25*, 730-748.
[121] P. Hoppe, S. Cohen, A. Meibom, *Geostand Geoanal Res* **2013**, *37*, 111-154.
[122] M. L. Kraft, P. K. Weber, M. L. Longo, I. D. Hutcheon, S. G. Boxer, *Science* **2006**, *313*, 1948-1951.
[123] F. Kollmer, W. Paul, M. Krehl, E. Niehuis, *Surf Interface Anal* **2013**, *45*, 312-314.
[124] A. Kubo, I. Ishizaki, A. Kubo, H. Kawasaki, K. Nagao, Y. Ohashi, M. Amagai, *Sci Rep-Uk* **2013**, *3*.
[125] A. van Remoortere, R. J. M. van Zeijl, N. van den Oever, J. Franck, R. Longuespee, M. Wisztorski, M. Salzet, A. M. Deelder, I. Fournier, L. A. McDonnell, *J Am Soc Mass Spectr* **2010**, *21*, 1922-1929.
[126] B. Spengler, M. Hubert, *J Am Soc Mass Spectr* **2002**, *13*, 735-748.
[127] A. Zavalin, J. Yang, K. Hayden, M. Vestal, R. M. Caprioli, *Anal Bioanal Chem* **2015**, *407*, 2337-2342.
[128] A. Rompp, B. Spengler, *Histochem Cell Biol* **2013**, *139*, 759-783.
[129] A. Venter, M. Nefliu, R. G. Cooks, *Trac-Trend Anal Chem* **2008**, *27*, 284-290.
[130] C. C. Hsu, P. T. Chou, R. N. Zare, *Anal Chem* **2015**, *87*, 11171-11175.
[131] J. Laskin, B. S. Heath, P. J. Roach, L. Cazares, O. J. Semmes, *Anal Chem* **2012**, *84*, 141-148.
[132] T. Cajka, O. Fiehn, *Trac-Trend Anal Chem* **2014**, *61*, 192-206.
[133] A. A. Makarov, E. N. Raptakis, P. J. Derrick, *International Journal of Mass Spectrometry and Ion Processes* **1995**, *146*, 165-182.
[134] J. S. Fletcher, S. Rabbani, A. Henderson, P. Blenkinsopp, S. P. Thompson, N. P. Lockyer, J. C. Vickerman, *Anal Chem* **2008**, *80*, 9058-9064.
[135] S. Wold, K. Esbensen, P. Geladi, *Chemometrics and Intelligent Laboratory Systems* **1987**, *2*, 37-52.
[136] M. S. Wagner, D. J. Graham, B. D. Ratner, D. G. Castner, *Surf Sci* **2004**, *570*, 78-97.
[137] B. J. Tyler, G. Rayal, D. G. Castner, *Biomaterials* **2007**, *28*, 2412-2423.
[138] E. S. F. Berman, L. G. Wu, S. L. Fortson, K. S. Kulp, D. O. Nelson, K. J. Wu, *Surf Interface Anal* **2009**, *41*, 97-104.
[139] C. Eriksson, P. Malmberg, H. Nygren, *Rapid Commun Mass Sp* **2008**, *22*, 943-949.
[140] G. A. Thompson, Jr., Y. Nozawa, *Biochimica et biophysica acta* **1977**, *472*, 55-92.
[141] M. P. Sauvant, D. Pepin, E. Piccinni, *Chemosphere* **1999**, *38*, 1631-1669.
[142] S. G. Ostrowski, C. T. Van Bell, N. Winograd, A. G. Ewing, *Science* **2004**, *305*, 71-73.
[143] M. E. Kurczy, P. D. Piehowski, C. T. Van Bell, M. L. Heien, N. Winograd, A. G. Ewing, *P Natl Acad Sci USA* **2010**, *107*, 2751-2756.
[144] R. J. Aitken, M. Q. Chaudhry, A. B. A. Boxall, M. Hull, *Occup Med-Oxford* **2006**, *56*, 300-306.
[145] T. Lowe, *Adv Mater Process* **2002**, *160*, 63-65.
[146] S. A. Carter, J. C. Scott, P. J. Brock, *Appl Phys Lett* **1997**, *71*, 1145-1147.
[147] C. O. Robichaud, A. E. Uyar, M. R. Darby, L. G. Zucker, M. R. Wiesner, *Environmental science & technology* **2009**, *43*, 4227-4233.
[148] R. Kaegi, A. Ulrich, B. Sinnet, R. Vonbank, A. Wichser, S. Zuleeg, H. Simmler, S. Brunner, H. Vonmont, M. Burkhardt, M. Boller, *Environmental Pollution* **2008**, *156*, 233-239.
[149] A. B. Boxall, K. Tiede, Q. Chaudhry, *Nanomedicine (Lond)* **2007**, *2*, 919-927.

[150] A. G. Cattaneo, R. Gornati, M. Chiriva-Internati, G. Bernardini, *Isj-Invert Surviv J* **2009**, *6*, 78-97.
[151] A. Kahru, H. C. Dubourguier, *Toxicology* **2010**, *269*, 105-119.
[152] N. S. Wigginton, K. L. Haus, M. F. Hochella, *Journal of Environmental Monitoring* **2007**, *9*, 1306-1316.
[153] D. B. Warheit, R. A. Hoke, C. Finlay, E. M. Donner, K. L. Reed, C. M. Sayes, *Toxicol Lett* **2007**, *171*, 99-110.
[154] A. Menard, D. Drobne, A. Jemec, *Environ Pollut* **2011**, *159*, 677-684.
[155] D. R. Baer, M. H. Engelhard, G. E. Johnson, J. Laskin, J. F. Lai, K. Mueller, P. Munusamy, S. Thevuthasan, H. F. Wang, N. Washton, A. Elder, B. L. Baisch, A. Karakoti, S. V. N. T. Kuchibhatla, D. Moon, *J Vac Sci Technol A* **2013**, *31*.
[156] R. D. Handy, R. Owen, E. Valsami-Jones, *Ecotoxicology* **2008**, *17*, 315-325.
[157] F. Draude, S. Galla, A. Pelster, J. Tentschert, H. Jungnickel, A. Haase, A. Mantion, A. F. Thunemann, A. Taubert, A. Luch, H. F. Arlinghaus, *Surf. Interface. Anal.* **2013**, *45*, 286-289.
[158] L. Yang, M. P. Seah, E. H. Anstis, I. S. Gilmore, J. L. S. Lee, *J. Phys. Chem. C* **2012**, *116*, 9311-9318.
[159] F. Kollmer, *Appl Surf Sci* **2004**, *231-232*, 153-158.
[160] D. Stapel, A. Benninghoven, *Appl Surf Sci* **2001**, *174*, 261-270.
[161] M. P. Seah, I. S. Gilmore, *Surf Interface Anal* **2011**, *43*, 228-235.
[162] A. G. Shard, S. Ray, M. P. Seah, L. Yang, *Surf. Interface. Anal.* **2011**, *43*, 1240-1250.
[163] A. G. Shard, R. Havelund, M. P. Seah, S. J. Spencer, I. S. Gilmore, N. Winograd, D. Mao, T. Miyayama, E. Niehuis, D. Rading, R. Moellers, *Anal. Chem.* **2012**, *84*, 7865-7873.
[164] P. J. Cumpson, J. F. Portoles, A. J. Barlow, N. Sano, *Journal of Applied Physics* **2013**, *114*.
[165] L. Yang, M. P. Seah, I. S. Gilmore, *J. Phys. Chem. C* **2012**, *116*, 23735-23741.
[166] J. S. Fletcher, S. Rabbani, A. M. Barber, N. P. Lockyer, J. C. Vickerman, *Surf. Interface. Anal.* **2013**, *45*, 273-276.
[167] C. Bich, R. Havelund, R. Moellers, D. Touboul, F. Kollmer, E. Niehuis, I. S. Gilmore, A. Brunelle, *Anal. Chem.* **2013**, *85*, 7745-7752.
[168] K. Moritani, G. Mukai, M. Hashinokuchi, K. Mochiji, *Surf. Interface. Anal.* **2011**, *43*, 241-244.
[169] M. P. Seah, *J Phys Chem C* **2013**, *117*, 12622-12632.
[170] K. Shen, A. Wucher, N. Winograd, *J Phys Chem C* **2015**, *119*, 15316-15324.
[171] P. Sjovall, B. Johansson, J. Lausmaa, *Appl Surf Sci* **2006**, *252*, 6966-6974.
[172] H. Nygren, K. Borner, P. Malmberg, B. Hagenhoff, *Appl Surf Sci* **2006**, *252*, 6975-6981.
[173] J. S. O'Brien, E. L. Sampson, *J Lipid Res* **1965**, *6*, 537-544.
[174] I. V. Bletsos, D. M. Hercules, D. Vanleyen, A. Benninghoven, C. G. Karakatsanis, J. N. Rieck, *Anal Chem* **1989**, *61*, 2142-2149.
[175] Y. Murayama, M. Komatsu, K. Kuge, H. Hashimoto, *Appl Surf Sci* **2006**, *252*, 6774-6776.
[176] C. L. Brummel, I. N. W. Lee, Y. Zhou, S. J. Benkovic, N. Winograd, *Science* **1994**, *264*, 399-402.
[177] M. Komatsu, Y. Murayama, H. Hashimoto, *Applied Surface Science* **2008**, *255*, 1162-1164.

[178] H. Nygren, P. Malmberg, *Proteomics* **2010**, *10*, 1694-1698.
[179] S. Lange, P. Malmberg, H. Nygren, *Surface and Interface Analysis* **2013**, *45*, 268-272.
[180] S. Vaidyanathan, M. Salim, C. Hurley, J. Pugh, *Surf Interface Anal* **2013**, *45*, 290-293.
[181] G. J. Currie, J. R. Yates, *J. Am. Soc. Mass Spectrom.* **1993**, *4*, 955-963.
[182] E. S. Lein, M. J. Hawrylycz, N. Ao, M. Ayres, A. Bensinger, A. Bernard, A. F. Boe, M. S. Boguski, K. S. Brockway, E. J. Byrnes, L. Chen, L. Chen, T. M. Chen, M. C. Chin, J. Chong, B. E. Crook, A. Czaplinska, C. N. Dang, S. Datta, N. R. Dee, A. L. Desaki, T. Desta, E. Diep, T. A. Dolbeare, M. J. Donelan, H. W. Dong, J. G. Dougherty, B. J. Duncan, A. J. Ebbert, G. Eichele, L. K. Estin, C. Faber, B. A. Facer, R. Fields, S. R. Fischer, T. P. Fliss, C. Frensley, S. N. Gates, K. J. Glattfelder, K. R. Halverson, M. R. Hart, J. G. Hohmann, M. P. Howell, D. P. Jeung, R. A. Johnson, P. T. Karr, R. Kawal, J. M. Kidney, R. H. Knapik, C. L. Kuan, J. H. Lake, A. R. Laramee, K. D. Larsen, C. Lau, T. A. Lemon, A. J. Liang, Y. Liu, L. T. Luong, J. Michaels, J. J. Morgan, R. J. Morgan, M. T. Mortrud, N. F. Mosqueda, L. L. Ng, R. Ng, G. J. Orta, C. C. Overly, T. H. Pak, S. E. Parry, S. D. Pathak, O. C. Pearson, R. B. Puchalski, Z. L. Riley, H. R. Rockett, S. A. Rowland, J. J. Royall, M. J. Ruiz, N. R. Sarno, K. Schaffnit, N. V. Shapovalova, T. Sivisay, C. R. Slaughterbeck, S. C. Smith, K. A. Smith, B. I. Smith, A. J. Sodt, N. N. Stewart, K. R. Stumpf, S. M. Sunkin, M. Sutram, A. Tam, C. D. Teemer, C. Thaller, C. L. Thompson, L. R. Varnam, A. Visel, R. M. Whitlock, P. E. Wohnoutka, C. K. Wolkey, V. Y. Wong, et al., *Nature* **2007**, *445*, 168-176.
[183] D. A. Berry, K. A. Cronin, S. K. Plevritis, D. G. Fryback, L. Clarke, M. Zelen, J. S. Mandelblatt, A. Y. Yakovlev, J. D. Habbema, E. J. Feuer, I. Cancer, C. Surveillance Modeling Network, *N Engl J Med* **2005**, *353*, 1784-1792.
[184] B. W. Stewart, C. Wild, International Agency for Research on Cancer, World Health Organization, *World cancer report 2014*, International Agency for Research on Cancer

WHO Press, Lyon, France

Geneva, Switzerland, **2014**.
[185] E. Gazi, J. Dwyer, N. Lockyer, P. Gardner, J. C. Vickerman, J. Miyan, C. A. Hart, M. Brown, J. H. Shanks, N. Clarke, *Faraday Discuss* **2004**, *126*, 41-59.
[186] J. W. Park, H. K. Shon, B. C. Yoo, I. H. Kim, D. W. Moon, T. G. Lee, *Appl Surf Sci* **2008**, *255*, 1119-1122.
[187] D. Debois, M. P. Bralet, F. Le Naour, A. Brunelle, O. Laprevote, *Anal Chem* **2009**, *81*, 2823-2831.
[188] S. Mas, D. Touboul, A. Brunelle, P. Aragoncillo, J. Egido, O. Laprevote, F. Vivanco, *Analyst* **2007**, *132*, 24-26.
[189] P. Malmberg, H. Nygren, K. Richter, Y. Chen, F. Dangardt, P. Friberg, Y. Magnusson, *Microsc Res Techniq* **2007**, *70*, 828-835.
[190] Y. Magnusson, P. Friberg, P. Sjovall, F. Dangardt, P. Malmberg, Y. Chen, *Clin Physiol Funct I* **2008**, *28*, 202-209.
[191] P. Malmberg, U. Bexell, C. Eriksson, H. Nygren, K. Richter, *Rapid Commun Mass Sp* **2007**, *21*, 745-749.
[192] B. M. Bluestein, F. Morrish, D. J. Graham, J. Guenthoer, D. Hockenbery, P. L. Porter, L. J. Gamble, *Analyst* **2016**, *141*, 1947-1957.
[193] F. P. Kuhajda, K. Jenner, F. D. Wood, R. A. Hennigar, L. B. Jacobs, J. D. Dick, G. R. Pasternack, *P Natl Acad Sci USA* **1994**, *91*, 6379-6383.
[194] F. Rohrig, A. Schulze, *Nat Rev Cancer* **2016**, *advance online publication*.

[195] S. C. Larsson, M. Kumlin, M. Ingelman-Sundberg, A. Wolk, *Am J Clin Nutr* **2004**, *79*, 935-945.
[196] J. Suburu, L. H. Shi, J. S. Wu, S. H. Wang, M. Samuel, M. J. Thomas, N. D. Kock, G. Y. Yang, S. Kridel, Y. Q. Chen, *Am J Physiol-Endoc M* **2014**, *306*, E1132-E1143.
[197] O. Warburg, *Naturwissenschaften* **1924**, *12*, 1131-1137.
[198] T. M. Loftus, D. E. Jaworsky, G. L. Frehywot, C. A. Townsend, G. V. Ronnett, M. D. Lane, F. P. Kuhajda, *Science* **2000**, *288*, 2379-2381.
[199] N. W. Chang, C. T. Wu, D. R. Chen, C. Y. Yeh, C. J. Lin, *J Nutr Biochem* **2013**, *24*, 274-281.
[200] E. Rysman, K. Brusselmans, K. Scheys, L. Timmermans, R. Derua, S. Munck, P. P. Van Veldhoven, D. Waltregny, V. W. Daniels, J. Machiels, F. Vanderhoydonc, K. Smans, E. Waelkens, G. Verhoeven, J. V. Swinnen, *Cancer Res* **2010**, *70*, 8117-8126.